Digital Control of Light

By

Nombuso Majola
207512837
BSc Hons (Physics)

A Thesis Submitted in Partial Fulfilment of the Requirement for the Degree Master of Science in Physics to the University of KwaZulu-Natal, School of Chemistry and Physics, Pietermaritzburg

Supervisor: Prof. N. Chetty [UKZN]
Co-Supervisors: Dr. A. Dudley [CSIR] and Prof. A. Forbes [WITS]

15 January 2019

Abstract

The objective of this research was to describe innovative ways in which digital holography can be applied in controlling laser light. The ability to control and manipulate a laser beam has become an extremely desirable feature since it enables improvement in the efficiency and quality of a number of applications.

Methods of controlling light make use of optical components to change the properties of a light beam according to the function of that optical element; therefore, a particular arrangement of optical elements in a system controls light in a certain way.

Technological advancements in the field of optics have developed a versatile device called a spatial light modulator (SLM), which is a novel instrument that employs computer generated holographic patterns (or phase masks) to modulate the amplitude and /or phase of a laser beam and it can therefore perform the function of a number of optical elements.

This research presents novel optical set-ups based on the phase-only liquid crystal spatial light modulator (LC-SLM) for generating, controlling and exploring different laser beam patterns. The thesis has three main sections, the first one is Holographic beam shaping, where a Gaussian beam was reshaped using an SLM to produce Vortex, Bessel or Laguerre-Gaussian beams. These beams were found to agree with theoretically generated beams.

Secondly, we produce off-axis laser beams by constructing coherent superpositions of Gaussian and vortex modes and then use two measurement techniques, peak intensity ratio and modal decomposition technique, to obtain the constituent components of these fields.

Finally, we investigate the propagation dynamics of Vortex and Laguerre-Gaussian beams by using a SLM to digitally propagate these beams in free space, and then perform measurements on the far field intensity pattern. The results show that the Laguerre-Gaussian beam suffers less spreading and beam distortion compared to the vortex beam in free space propagation.

Declaration

This thesis describes the work undertaken at the University of KwaZulu-Natal (Pietermaritzburg) and the Council for Scientific and Industrial Research (CSIR), Pretoria under the supervision of Prof. N. Chetty, Dr. A. Dudley and Prof. A. Frobes between February 2013 and March 2018.

I (Nombuso Majola, 207512837) declare the work reported herein to be my own research, unless specifically indicated to the contrary in the text. MatLab codes for producing holograms were written by Dr. A Dudley, and modified by the author to produce holograms required by a particular experiment.

Signed:.....
On this.....day of.....2018.

I hereby certify that this statement is correct

.....
Prof. N. Chetty (Main-Supervisor)

.....
Dr. A. Dudley (Co-Supervisor)

.....
Prof. A. Forbes (Co-Supervisor)

Publications

1. A. Dudley, N. Majola, N. Chetty, and A. Forbes, "Implementing digital holograms to create and measure complex-plane optical fields", Am. J. Phys. 84, 106-112 (2016)

Contents

Acknowledgements

I would like to gratefully thank my supervisors Prof. Chetty, Dr. Dudley and Prof. Forbes for their assistance and guidance during this project and also for helpful corrections of the thesis.

I would also like to acknowledge the Council for Scientific and Industrial Research (CSIR), National Laser Center (NLC) for allowing me the opportunity to conduct the experimental part of this work. Financial support from the National Research Foundation (NRF) and the University of KwaZulu-Natal, College of Science and Agriculture is gratefully acknowledged.

Last but not least, my family and friends for support, patience and encouragement when it was needed.

1 Introduction

Optics is the branch of physics which involves the behavior and properties of light including its interaction with matter and the construction of instruments that control, use or detect it [1]. The need for controlling light has arisen in many fields of scientific, engineering and industrial research and development [2]. It has also become an important part of astronomy [3]. These applications use lasers since they offer a coherent and monochromatic source of energy.

A wide variety of techniques have been developed, applied and tested by researchers to control light. Methods used before the late 1940's employed the traditional optical elements such as mirrors, lenses, etc.; to control light. These components were made with various types of glass and therefore are fixed to performing a particular function; as a result, an arrangement of optical elements in a system is limited to controlling light in a certain way and changing the system to perform another function is time consuming. Furthermore, many optical components need to be used in a given application therefore increasing the sources of errors in a system and the associated costs.

Optical technological innovations and the use of computer controlled devices are observable and have provided solutions in various fields. They have been applied as a way of addressing challenges and therefore improving the operation of certain systems [5]. In optics, technological advancements have resulted in the creation of holographic optical elements (HOEs); these are lenses, mirrors, gratings prisms, beam splitters,etc., made by holographic methods [6]. These optical elements obey the rules of geometrical optics and can be used for any purpose that conventional optical elements were used for, with the provision that they operate efficiently over a narrow band of wavelengths [7]. HOEs have provided new methods to control the intensity, phase and polarization of laser light.

The combination of holography and liquid crystal micro-display technology have resulted in the fabrication of a device called a spatial light modulator (SLM). The term spatial light modulator is used to describe a computer controlled liquid crystal device that consists of an array of pixels, each of which can modulate the amplitude, phase, or polarization of light waves passing through it or reflected from it, in both space and time [8]. The SLM can be encoded with different digital holograms and can perform the function of any optical element in manipulating the properties of a laser beam; and in this way digital control of light is achieved.

Applications of a digital light controlling system are unlimited. It can be used to improve the quality of a certain system, or to ease carrying out a certain experiment or achieving a certain level of accuracy. As an example, Schulze et. al. [9], and Pérez-Vizcaíno et. al. [10], made use of an SLM for the ease of performing the measurement of the laser beam propagation factor (M2); electronically tunable focal length lenses were used without moving components in contrast to the standard procedure described in ISO/DIS 11146 which requires physical movement of the camera for mechanical scanning of the laser beams propagation path. In optical tweezing, SLMs and digital holography technologies provide a tool to control and manipulate multiple particles at the same time [11], [12].

It is also possible to digitally reshape a laser beam by using an SLM [13], this has the advantage that laser beam shapes are created to meet the requirements of a particular application [14], [15]. The benefit is that many laser beam shapes can be achieved by using a single laser beam. Furthermore, the versatility of the SLM also allows simulation of digital free space propagation [10] and propagation through turbulence [16] .

Light is radiant energy; this is the electromagnetic (EM) radiation that can be detected by the human eye. Historical developments in optics revealed that light has the form of an electromagnetic wave [17], [18]. When James Clerk Maxwell was studying the equations describing electric and magnetic fields, in 1865 in Scotland he found that the speed of an electromagnetic wave should be the same as the speed of light, within experimental error [19]. Electromagnetic waves are fluctu-

ations of electric and magnetic fields, which can transport energy from one location to another.

The objective of this thesis is to describe innovative ways in which digital holography technology can be applied in controlling laser light. The rest of this thesis is organized as follows; In Chapter 2, we recap some fundamental results from optics that are important for this thesis, we briefly cover Maxwell's equations and then give the derivation of the paraxial Helmholtz equation from Maxwell's equations. Chapter 3 presents the general aspect of holographic beam shaping; the tools that can be used to realize holographic beam shaping as well as the theory of the beams that will be constructed. In Chapter 4 we present the theory behind off-axis vortex beams and also the results of the experiment. A study of the propagation dynamics of Vortex and LG beams is presented in Chapter 5. A conclusion is given in Chapter 6, after which appendices follow.

2 Theoretical Background

In this chapter we present the theory that the research in this thesis was based. The propagation of light waves is described by the wave equation, which can be derived from Maxwell's equations. If the propagation direction of a light wave is well defined, which is the case for laser beams, the paraxial approximation can be applied, giving rise to the paraxial wave equation [20]. We will derive the wave equation from Maxwell's equations, and then apply the paraxial approximation to obtain the paraxial Helmholtz wave equation. The mathematical equations that describe the Gaussian beam, Laguerre-Gauss beams and Bessel gauss beams are also derived in this section. These equations have important results that give us the basic understanding of light fields and their propagation characteristics [21].

2.1 Maxwell's Equations

Light is an electromagnetic wave and the propagation of electromagnetic waves in free space can be described by the wave equation. Maxwell's equations govern electromagnetic fields, and also form the foundation of the Helmholtz wave equation . As a consequence, the derivation of the wave equation begins with Maxwell's equations in a vacuum, given by the following set of partial differential equations [22];

$$\nabla \cdot \vec{E} = 0 \tag{1}$$

$$\nabla \cdot \vec{B} = 0 \tag{2}$$

$$\nabla \times \vec{E} = -\frac{\partial \vec{B}}{\partial t} \tag{3}$$

$$\nabla \times \vec{B} = \epsilon_0 \mu_0 \frac{\partial \vec{E}}{\partial t}. \tag{4}$$

In these equations $\vec{E}$ is the electric field, $\vec{B}$ is the magnetic field, and ϵ_0 and μ_0 are the permittivity and the permeability of free space, respectively. Equations (1) and (2) are called Gauss' law for electric and magnetic fields, and equations (3) and (4) are called Faraday's law and Amperès law, respectively [23].

2.2 The derivation of the Wave Equation

The wave equation is derived from Maxwell's equations. Taking the curl of Faraday's law, equation (3), and then changing the order of differentiation on the right-hand side provides:

$$\nabla \times (\nabla \times \vec{E}) = -\frac{\partial (\nabla \times \vec{B})}{\partial t}. \tag{5}$$

Substituting Amperès law, equation (4) into equation (5), and using the fact that the constants ϵ_0 and μ_0 are both independent of time, it can be shown that:

$$\nabla \times (\nabla \times \vec{E}) = -\epsilon_0 \mu_0 \frac{\partial^2 \vec{E}}{\partial t^2}. \tag{6}$$

Applying the following identity from vector calculus [24]:

$$\nabla \times (\nabla \times \vec{E}) = \nabla \cdot (\nabla \cdot \vec{E}) - \nabla^2 \vec{E}, \tag{7}$$

which states that the double-curl operation on a vector may be rewritten as a gradient-divergence and a Laplacian operation [25], into equation (6) produces:

$$\nabla \cdot (\nabla \cdot \vec{E}) - \nabla^2 \vec{E} = -\epsilon_0 \mu_0 \frac{\partial^2 \vec{E}}{\partial t^2}. \tag{8}$$

Applying Gauss' law, (equation (1)), to equation (8) makes the first term zero and the equation becomes,

$$\nabla^2 \vec{E} - \epsilon_0 \mu_0 \frac{\partial^2 \vec{E}}{\partial t^2} = (\nabla^2 - \epsilon_0 \mu_0 \frac{\partial^2}{\partial t^2})\vec{E} = 0, \tag{9}$$

which is the wave equation. Another equation for the magnetic field can be derived using a similar approach, taking the curl of equation (4) and substituting equations (2) and (3) :

$$\nabla^2 \vec{B} - \epsilon_0 \mu_0 \frac{\partial^2 \vec{B}}{\partial t^2} = (\nabla^2 - \epsilon_0 \mu_0 \frac{\partial^2}{\partial t^2})\vec{B} = 0. \tag{10}$$

Both equations (9) and (10) have the form of a general wave equation for a wave traveling with velocity $c = \frac{1}{\sqrt{\epsilon_0 \mu_0}} = 3 \times 10^8 m \cdot s^{-1}$.

2.3 Derivation of Helmholtz Wave Equation

The Helmholtz wave equation is the partial differential equation [26]:

$$\nabla^2 A + k^2 A = 0, \tag{11}$$

where $\nabla^2 = \frac{\partial^2}{\partial x^2} + \frac{\partial^2}{\partial y^2} + \frac{\partial^2}{\partial z^2}$ is the Laplacian operator, k is the wave number and A is the amplitude. The Helmholtz wave equation is the time independent form of the wave equation and can be derived by applying a method of separation of variables to the wave equation. Consider the scalar wave equation;

$$\left(\nabla^2 - \frac{1}{c^2}\frac{\partial^2}{\partial t^2}\right) U(\vec{r}, t) \tag{12}$$

where the scalar function $U(\vec{r}, t)$ (which depends on both space and time) represents the amplitude of an electromagnetic wave propagating in free space, c is the vacuum speed of light, $\vec{r} = (x, y, z)$ represents position in three dimensional space and t represents time. Suppose that the wave function $U(\vec{r}, t)$ is separable, i.e. is given by;

$$U(\vec{r}, t) = A(\vec{r})T(t). \tag{13}$$

Substituting this separable wave function into the wave equation (12) and simplifying, we obtain:

$$\frac{\nabla^2 A}{A} = \frac{1}{c^2 T}\frac{\partial^2 T}{\partial t^2}. \tag{14}$$

The expression on the left-hand side depends only on $\vec{r}$, whereas the right hand side of the equation depends only on t. This equation is valid if and only if both sides of the equation are equal to a constant. From this observation, we obtain two equations, one for $A(\vec{r})$, and the other for T(t):

$$\frac{\nabla^2 A}{A} = -k^2, \tag{15}$$

and

$$\frac{1}{c^2 T}\frac{\partial^2 T}{\partial t^2} = -k^2, \tag{16}$$

where we have chosen $-k^2$ as a constant. Re-arranging the first equation, we obtain:

$$\nabla^2 A + k^2 A = (\nabla^2 + k^2)A = 0, \tag{17}$$

This is the spatial Helmholtz wave equation, and it provides solutions that describe the propagation of waves in free space.

2.4 The Paraxial Approximation

The spatial Helmholtz equation is widely used in optics and most applications rely on the paraxial approximation because numerical solutions to the paraxial wave equation can be generated numerically and are simple to implement [27]. In this section we will derive the paraxial approximation of the Helmholtz wave equation. The light beam's complex magnitude of the electric field can be written in the form,

$$E(x,y,z) = U(x,y,z)exp(ikz), \tag{18}$$

where $U(x,y,z)$ is the complex valued amplitude of the electric field, which modulates the sinusoidal plane wave by the exponential factor $exp(ikz)$, and z is the propagation axis. The paraxial form of the Helmholtz equation is found by substituting the above complex magnitude of the electric field into the general form of the Helmholtz equation as follows:

$$\nabla^2 E(x,y,z) + k^2 E(x,y,z) = \nabla^2 U(x,y,z)exp(ikz) + k^2 U(x,y,z)exp(ikz) = 0 \tag{19}$$

Expanding the Cartesian Laplacian and differentiating the longitudinal component gives,

$$\left(\frac{\partial^2}{\partial x^2} + \frac{\partial^2}{\partial y^2} + \frac{\partial^2}{\partial z^2}\right)U(x,y,z)exp(ikz) + k^2 U(x,y,z)exp(ikz) = 0 \tag{20}$$

$$\begin{aligned}\left(\frac{\partial^2}{\partial x^2} + \frac{\partial^2}{\partial y^2}\right)U(x,y,z)exp(ikz) + \frac{\partial^2}{\partial z^2}U(x,y,z)exp(ikz) \\ + k^2 U(x,y,z)exp(ikz) = 0,\end{aligned} \tag{21}$$

and

$$\begin{aligned}exp(ikz)\left(\frac{\partial^2}{\partial x^2} + \frac{\partial^2}{\partial y^2}\right)U(x,y,z) + exp(ikz)\left(\frac{\partial^2}{\partial z^2} + 2ik\frac{\partial}{\partial z} - k^2\right)U(x,y,z) \\ + k^2 U(x,y,z)exp(ikz) = 0.\end{aligned} \tag{22}$$

Removing the complex exponential factors, and since the "k^2" terms sum up to zero we obtain,

$$(\frac{\partial^2}{\partial x^2} + \frac{\partial^2}{\partial y^2} + \frac{\partial^2}{\partial z^2})U(x,y,z) + 2ik\frac{\partial U(x,y,z)}{\partial z} = 0. \tag{23}$$

This is the Helmholtz equation without the approximation. The paraxial approximation is defined by the condition:

$$\frac{\partial^2 U(x,y,z)}{\partial z^2} << k\left|\frac{\partial U(x,y,z)}{\partial z}\right|, \tag{24}$$

which means that the longitudinal variation in the modulation function $U(x,y,z)$ changes very slowly in distance compared to the wavelength $\lambda = \frac{2\pi}{k}$, of the beam. This approximation enables us to neglect the longitudinal derivative term, $\frac{\partial^2 U(x,y,z)}{\partial z^2}$, in equation (23) so that we get the expression,

$$\nabla_\perp^2 U(x,y,z) + 2ik\frac{\partial U(x,y,z)}{\partial z} = 0, \tag{25}$$

where $\nabla_\perp^2 = \frac{\partial^2}{\partial x^2} + \frac{\partial^2}{\partial y^2}$ is the transverse part of the Laplacian. This expression is called the paraxial approximation of the Helmholtz wave equation.

2.5 Mathematical Functions Describing Optical Beams

Many explanations in science make use of mathematical equations to explain in some detail a physical phenomena; therefore mathematical equations that describe light beams have been formulated; these equations give the basic understanding of light fields.

A Helium Neon (HeNe) laser was used as the optical beam source in all the research presented in this thesis. A laser is a device that emits an intense beam of coherent, directional and monochromatic light (or EM radiation). The first successful laser was invented in 1960 by Theodore H. Maiman [28, 29]. A laser is constructed from three principal parts; an energy source, a gain medium and two mirrors that form an optical resonator. The geometrical characteristics of the resonator mirrors determine the type and shape of laser emission obtained [37].

Unguided EM waves in free space can be described as a superposition of plane waves. However, if there are boundary conditions imposed by a physical structure, a wave can be described in terms of transverse modes. A transverse mode of a beam of EM radiation is a particular pattern of intensity distribution across the width of the beam measured in a plane perpendicular (i.e. transverse) to the propagation direction of the beam [30]. The transverse modes are consequential of the boundary conditions imposed on the wave by a wave-guide, i.e. any device or structure that encloses and guides waves between its end points.

Inside the laser cavity, the laser's radiation is guided between the mirrors of the laser resonator. They may have either a plane or have curved surface, (e.g. cylindrical or spherical). Therefore a laser's radiation is characterized by transverse modes which arise from the boundary conditions imposed through the resonator mirrors shape.

Most common optical beams emitted by a laser source obey the Paraxial wave equation [31]. We are interested in laser beams which are solutions to the paraxial wave equation because they are transverse Eigen modes of stable resonators and they are structurally stable, i.e., they do not change shape on propagation [32]. This quality enables one to achieve less distortions compared to other sources. Equations describing the laser modes that were investigated are derived below, starting from the lower order (TEM_{00}) mode; the Gaussian beam.

2.5.1 The Gaussian Beam

A Gaussian beam is a beam of electromagnetic radiation whose transverse electric field and intensity (irradiance) distributions are well approximated by the Gaussian function. It is produced by lasers operating in the fundamental transverse electromagnetic mode (TEM_{00}) of the laser resonator. The radial and transverse profiles of the Gaussian beam are depicted by Figures 1(a) and 1(b) respectively.

The light beam produced by most lasers offers a highly directional and localized source of energy [33], and maintains its shape and size over long distances [34]. These properties make laser light well suited for use at precise locations, and therefore exceedingly useful for a variety of applications such as drilling, cutting, welding, surgery in medicine, communication in fibre optics, etc. In addition to that, the Fourier transform of a Gaussian intensity profile remains a Gaussian and thus preserves it shape as it passes through an optical system consisting of simple lenses. This is important when multiple optical elements are employed to guide the laser radiation [35].

The Gaussian beam is the lowest order solution in an infinite family of solutions for the free space paraxial wave equation [36]. The Gaussian beam has a field mathematically expressed as;

$$U(r,z) = \frac{\omega_0}{\omega\,(z)} exp\left(\frac{-r^2}{\omega^2(z)}\right) exp\left(-ik\frac{r^2}{2R(z)} - i\phi(z)\right), \tag{26}$$

where,

$$\omega(z) = \sqrt{\omega_0^2 \left(1 + \frac{z^2}{Z_R}\right)}, \tag{27}$$

is the radius at which the amplitude decreases by a factor of e^{-1} and is termed the beam radius.

Figure 1: The radial (a) and the transverse (b) intensity of a Gaussian beam.

The beam radius varies with propagation distance but it is a minimum at only one point along the beam profile; this narrowest point is denoted by ω_0, and is called the beam waist. Z_R is the Rayleigh range and $R(z)$ is the radius of curvature of the wavefront, and is given by [37]:

$$R(z) = z \left(1 + \frac{z^2}{Z_R}\right) \tag{28}$$

The gouy phase is given by [37]:,

$$\phi(z) = tan^{-}1 \left(\frac{z^2}{Z_R}\right). \tag{29}$$

The beam divergence in the far field (i.e., for z values much larger than Z_R) is

$$\theta = \frac{\lambda}{\pi\omega_0}. \tag{30}$$

The set of parameters described above govern the geometry and behavior of the field of a Gaussian beam as it propagates in free space, and are also illustrated by Figure 2. The intensity of a Gaussian beam is given by the square modulus of the amplitude distribution, and varies with radial distance r from the axis as,

$$I(r,z) = |U(r,z)|^2 = (\frac{\omega_0}{\omega(z)})^2 exp(\frac{-2r^2}{\omega^2(z)}). \tag{31}$$

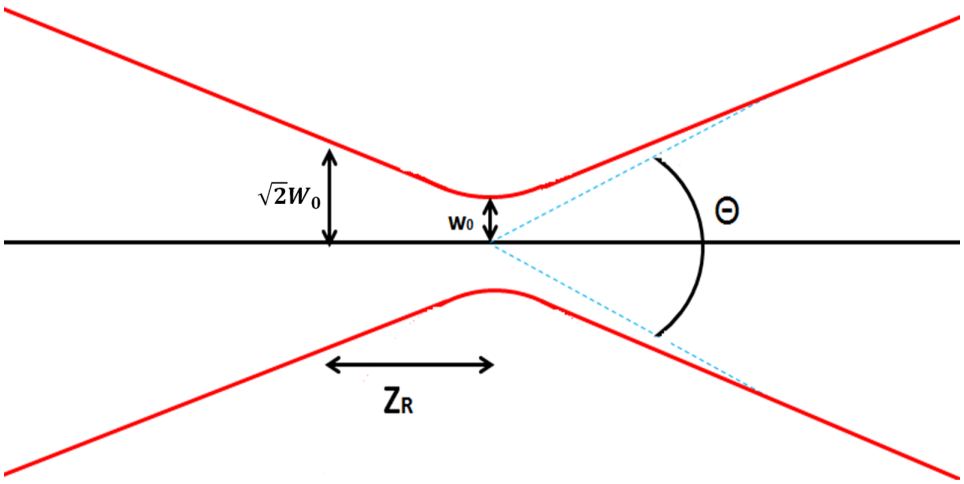

Figure 2: The Gaussian beam width $\omega(z)$ as a function of propagation distance z along the beams propagation axis. The characteristic parameters that govern the geometry and behavior of the beam are: beam waist, ω_0, Rayleigh range, Z_R, and total angular spread, θ.

2.5.2 Laguerre-Gaussian Beam

Laguerre-Gaussian modes are another set of functions which are solutions to the paraxial wave equation. These modes are a particular class of cylindrically symmetric laser modes. They are defined in cylindrical coordinates and the complex amplitude distribution of the field of an LG_{pl} mode propagating along the z-axis is mathematically expressed as [38], [39]:

$$U_{p,l}(r,\phi,z) = \frac{1}{\omega(z)}\sqrt{\frac{2p!}{\pi(|l|+p)!}}exp\Big[i(2p+|l|+1)\psi(z)\Big] \times \left(\frac{\sqrt{2}r}{\omega(z)}\right)^{|l|} \times L_p^l\Big(\frac{2r^2}{\omega^2(z)}\Big)exp\Big[-ik\frac{r^2}{2q(z)}+il\phi\Big], \tag{32}$$

where (r,ϕ,z) are cylindrical coordinates around the optical axis and k is the wave number. The LG mode is characterized by two integer indices, the azimuthal index l that correspond to the topological charge of the optical vortex, and the radial index p that defines the number of radial nodes of the mode. $L_p^l(x)$ is the generalized Laguerre polynomial that gives LG modes their characteristic ring shape. Examples of LG modes are given in Figure 4. The Gouy phase of an LG beam is defined by [39]:

$$\phi(p,l,z) = (2p+l+1)arctan(\frac{z}{z_R}). \tag{33}$$

All other parameters are defined the same way as they are for Gaussian beams. The most interesting term is the one containing the azimuthal phase (i.e., $exp(il\phi)$), and is responsible for their orbital angular momentum of $l\hbar$ per photon [40]. Points of constant phase (i.e. the wave front) form a helix and the wave front consist of l intertwined helices. The LG_{pl} solution reduces to the zero-order solution (Gaussian) when $p = l = 0$. When $l \neq 0$ and $p = 0$ the LG beam has an intensity distribution given by:

$$I(r,\theta) = \frac{2}{\pi\omega^2 l!}\left(\frac{r\sqrt{2}}{\omega}\right)^{2l} exp\left(\frac{2r^2}{\omega^2}\right), \tag{34}$$

where l is the topological charge of the vortex and ω is the width of the Gaussian envelope. The intensity distribution is a single-ringed doughnut shape, depicted by Figure 3. The maximum intensity is found at a radial distance [41]:

$$r_{max} = \frac{\sqrt{2}}{2}\omega\sqrt{l}, \tag{35}$$

from the symmetry axis of an LG mode and depends on l as

$$I(r_{max}) = \frac{2}{\pi\omega^2 l!}l^l e^{-l}. \tag{36}$$

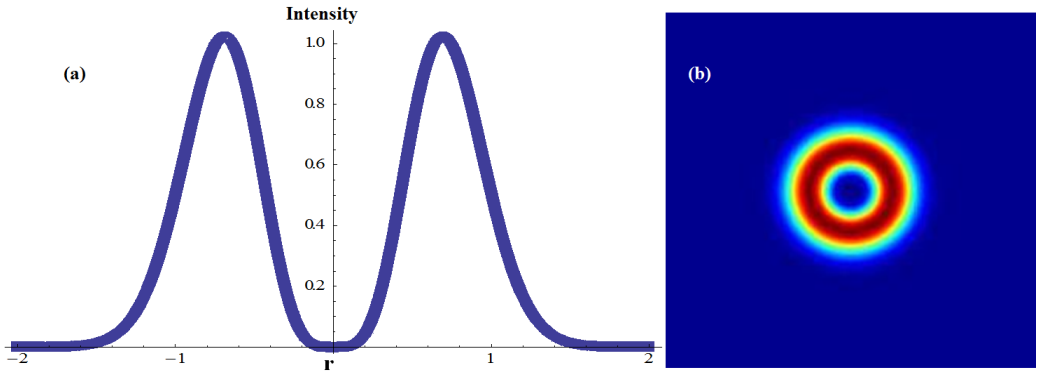

Figure 3: The radial (a) and transverse (b) intensity profile for $p = 0$ and $l = 1$, LG mode.

For large values of topological charge, $I(r_{max})$ decreases as the inverse of the square root of l.

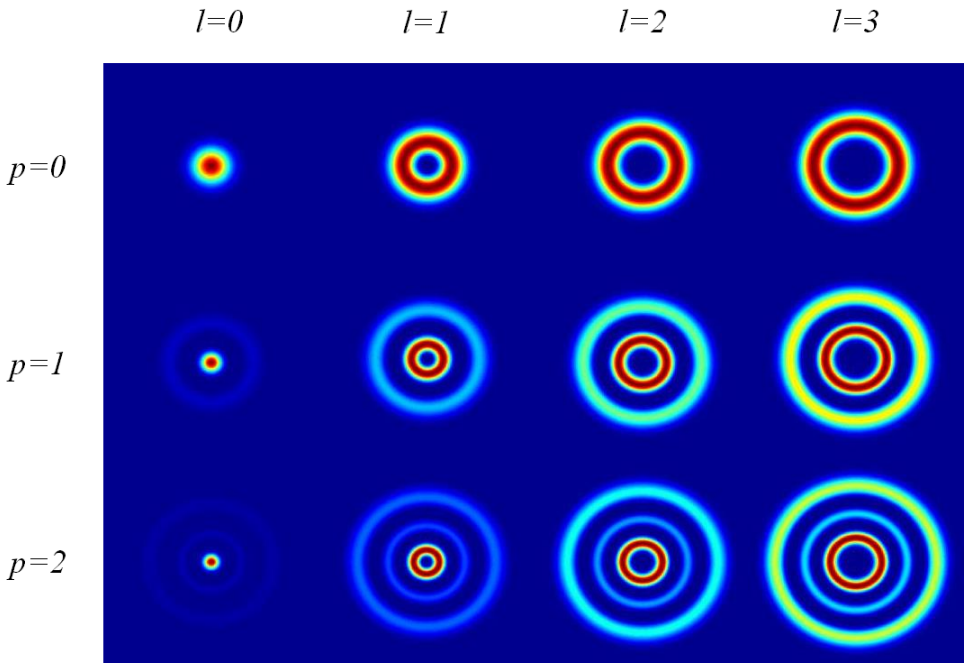

Figure 4: The transverse modes of Laguerre Gaussian beams generated with various l and p indices.

2.5.3 Bessel Beams

Another set of solutions to the wave equation are the so called "diffraction-free" Bessel beams [42]. A Bessel Beam is a field of electromagnetic radiation whose amplitude is described by a Bessel function of the first kind, and is given by the expression:

$$U(r,\phi,z) = A\frac{\omega_0}{\omega(z)}exp\left[i\left(k-\frac{k_r^2}{2k}\right)z - i\phi(z) + il\theta\right] \times J_l\left(\frac{k_r r}{i\frac{z}{z_R}}\right) \times exp\left[\left(\frac{-1}{\omega^2(z)} + \frac{ik}{2R(z)}\right)\left(r^2 + \frac{k_r^2 z^2}{k^2}\right)\right], \tag{37}$$

where J_l is the l^{th} order Bessel function, k_z and k_r are the longitudinal and radial wave vectors, with $k = \sqrt{k_z^2 + k_r^2} = \frac{2\pi}{\lambda}$, λ is the wavelength of electromagnetic radiation making up the Bessel beam, and r, ϕ and z are the radial, azimuthal and longitudinal components respectively.

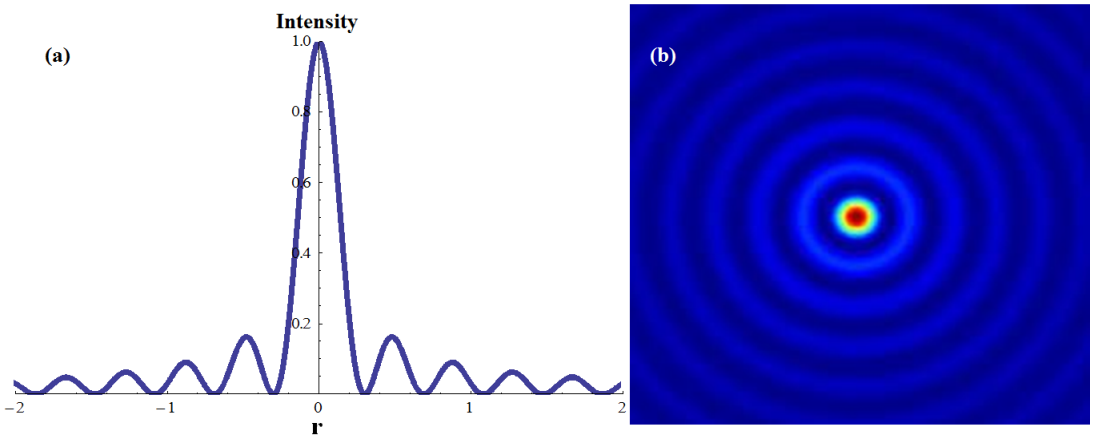

Figure 5: The radial (a) and transverse (b) pattern of a zeroth order Bessel-Gauss beam.

The intensity of a zeroth order ($l = 0$) Bessel beam has a central circular disk surrounded by a pattern of a ring(s), shown in Figure 5. The beams described by higher order functions ($l > 0$), an example given in Figure 6, are called high order Bessel beams (HOBBs) and have a phase singularity on the beam axis and hence a dark core [46].

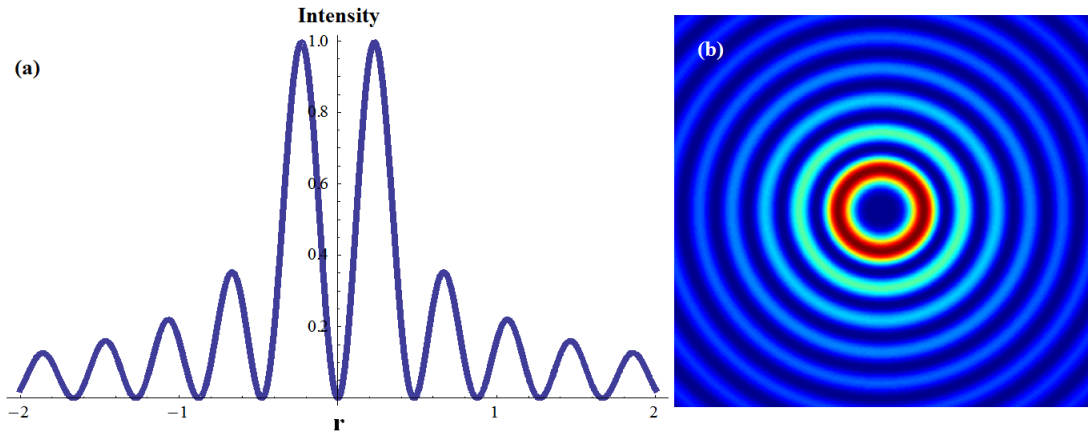

Figure 6: The radial (a) and transverse (b) pattern of a third order Bessel-Gauss beam.

2.6 Summary

Fundamental results of optics that are relevant to this work have been presented, starting from Maxwell's equations to the derivation of the paraxial Helmholtz wave equation. The mathematical equations of selected types of laser beam modes have been presented because they give the basic properties of light fields and their propagation characteristics. The novel laser beams introduced are optical Laguerre-Gaussian beams and Bessel beams. The vortex beam has a doughnut shaped transverse intensity pattern, and is similar to that of the LG mode, the difference is that the vortex mode depends only on the azimuthal index l, and the LG mode depends on both the radial p, and azimuthal l, indices. The transverse profile of the Bessel beam consist of a pattern of concentric rings.

References

[1] W. J. Smith, Modern Optical Engineering, 3^{rd} Ed., The McGraw-Hill Companies, Inc, USA (2000).

[2] F. M. Dickey, L. S. Weichrnan, R. N. Shagam (2000, April 4). Laser Beam Shaping Techniques, Retrieved from http://www.osti.gov/scitech/servlets/purl/752659.

[3] C. Béchet, A. Guesalaga, B. Neichel, V. Fesquet, H. González-Núñez, S. Zúñiga, P. Escarate, and D. Guzman, Beam shaping for laser-based adaptive optics in astronomy, Optics Express, Vol. 22, Issue 11, pp. 12994-13013 (2014).

[4] A. Jesacher, C. Maurer, A. Schwaighofer, S. Bernet and M. Ritsch-Marte, Near-perfect hologram reconstruction with a spatial light modulator, Optical Society of America, Vol. 16, No. 4 (2008).

[5] E. F. Camacho, T. Samad, M. Garcia-Sanz and I. Hiskens. "Control for renewable energy and smart grids", Chapter in "The Impact of Control Technology", T. Samad, A.M. Annaswamy (eds.), IEEE - Control Systems Society, 2011.

[6] G. Hedge, Holography and Its Applications, Available online: http://nitksummerschool.yolasite.com/resources/Holography

[7] K. E. Olsen, Holographic multi-stereogram constructed from computer images: Applied 3-D printer, Cand. scient. thesis in Optics and Laser Physics, Department of Physics, UoB, May 1996.

[8] G. Lazarev, A. Hermerschmidt, S. Kruger, and S. Osten, LCOS Spatial Light Modulators: Trends and Applications, available online, accessed at: http://www.wiley-vch.de/books/sample/3527410643_c01.pdf.

[9] C. Schulze, D. Flamm, M. Duparré, and A. Forbes, Beam-quality measurements using a spatial light modulator, Optics Letters, Vol. 37, Issue 22, pp. 4687-4689 (2012).

[10] J. Pérez-Vizcaíno, O. Mendoza-Yero, R. Martínez-Cuenca, L. Martínez-León, E. Tajahuerce and J. Lancis, Free-Motion Beam Propagation Factor Measurement by Means of a Liquid Crystal Spatial Light Modulator, GROC, Institute of New Imaging Technologies, Universitat Jaume I, 12071-Castelló, Spain.

[11] R. L. Eriksen, V. R. Daria and J. Glückstad, Fully Dynamic Multiple-Beam Optical Tweezers, Opt. Eepress 597, No. 14, Vol 10, 2002.

[12] D. McGloin, D. R. Burnham, M. D. Summers, D. Rudd, N. Dewara and S. Anand, Optical Manipulation of Airborne Particles: Techniques and Applications, Faraday Discuss., 2008, 137, 335–350.

[13] S.Ngcobo, I. Litvin, L. Burger and A. Forbes, A digital laser for on-demand laser modes, Nature Communications volume 4, Article number: 2289 (2013).

[14] Z. Kuang, J. Li, S. Edwardson, W. Perrie, D. Liu and G. Dearden, Ultrafast laser beam shaping for material processing at imaging plane by geometric phase masks using a spatial light modulator, accessed at: https://livrepository.liverpool.ac.uk/3002110/1/OLE

[15] D. Preece, R. Bowman, G. Gibson and M. Padgett, A comprehensive software suite for optical trapping and manipulation, Proc. of SPIE Vol. 7400 74001N-1.

[16] K. Drexler , M. Roggemann and D, Voelz, Use of a Partially Coherent Transmitter Beam to Improve the Statistics of Received Power in a Free-Space Optical Communication System: Theory and Experimental results, Opt. Eng. 50(2), 025002 (February 03, 2011).

[17] H. D. Young and R. A. Freedman, University Physics with Modern Physics (14th Edition), Pearson Education Limited, 2016.

[18] L. J. Vandergriff, Fundamental of Photonics, Module 1.1, accessed at:https://spie.org/Documents/Publications/00

[19] R. Jennny, Fundamental of Optics-An Introduction for beginners, Available online, exceed at: http://www.vision-systems.com/articles/print/volume-6/issue-2/back-to-basics/fundamentals-of-optics-an-introduction-for-beginners.html.

[20] M. Lax, W. H. Louisell, and W. B. McKnight, 'From Maxwell to Paraxial Wave Optics', Phys. Rev. A 11, 1365 (1975).

[21] H. Kogelnik and T. Li, Laser Beams and Resonators, J. Applied Optics, Vol. 5, Issue 10, pp. 1550-1567 (1966).

[22] D. Fleisch, A Student's Guide to Maxwell's Equations, Cambridge University Press, New York, 2008.

[23] A. Bamberger, B. Engquist, L. Halpern and P. Joly, Higher Order Paraxial Wave Equation Approximations in Heterogeneous Media, SIAM Journal of Applied Mathematics (1998), Pages 129-154.

[24] T. L. Chow, Mathematical Methods for Physicists: A concise introduction,Cambridge University Press(Virtual Publications), 2003.

[25] Notes on Wave Equations, available online:
//www.propagation.gatech.edu/ECE3025/opencourse/WAV/$EmagNotes_WaveEquations$.pdf

[26] B. E. A. Saleh, M. C. Teich, Fundamentals of Photonics (Second Edition), John Wiley and Sons, Inc., New Jersey, 1991.

[27] A. J. Turska, B. Atamaniuk and E. Turska, Fractional Derivative Analysis of Helmholtz and Paraxial-Wave equations, Department of Theory of Continuos Mechanics, Institute of Fundamental Technological Research, PAS, 2002.

[28] Available online, accessed at:
http://inventors.about.com/od/lstartinventions/a/laser.htm.

[29] Available online, accessed at:
http://www.worldoflasers.com/laserhistory.htm .

[30] J. Hecht, Understanding Lasers: An Entry-Level Guide,3^{rd} Edition, John Wiley and Sons, Inc., New Jersey, 2008.

[31] E. Karimi and E. Santamato, Radial coherent and intelligent states of the oparaxial wave equation, , J. Opt. Soc. Am.,2013: available online at: http://arxiv.org/pdf/1211.4162v1.pdf.

[32] M. A. Bandres, and J. C. Gutiérres-Vega, Ince-Gaussian Modes of the Paraxial Wave Equation and Stable Resonators, J. Opt. Soc. Am., No. 5, Vol. 21, 2004.

[33] J. Wilson and J. F. B. Hawkes(eds.) Laser Principles and Applications (Prentice Hall International, Hertfordshire, UK, 1987).

[34] Available online, excessed at: http://www.infoplease.com/encyclopedia/science/laser-applications-lasers.html.

[35] M. Duocastella and C. B. Arnold, Bessel and annular beams for material processing, Laser Photonics Rev.6, No.5, 607-621 (2012).

[36] B. Liu, Optimal Beam Forming for Laser Beam Propagation Through Random Media, PhD Dissertation, Michigan Technological University (2006).

[37] J. Alda, Laser and Gaussian Beam Propagation and transformation, Encyclopedia of optical engineering, Marcel Dekker, New York, 2003.

[38] S. A. Kennedy, M. J. Szabo, H. Teslow, J. Z. Porterfield, and E. R. I. Abraham, Phys. Rev. A 66, 043801 (2002).

[39] J.Hamazaki, Y. Mineta, K. Oka and R. Morita, Direct observation of Gouy Phase Shift in a Propagating Optical Vortex, OPTICS EXPRESS 8382, Vol. 14, No. 18, 2006.

[40] L. Allen, M. W. Beijersbergen, R. J. C. Spreeuw, and J. P. Woerdman, 1992, Phys. Rev. A, 45, 8185.

[41] M.J Padgett, F. M Miatto, M. P. J. Lavery, A. Zeilinger and R. W. Boyd, Divergence of an orbital-angular-momentum-carrying beam upon propagation, New J. Phys. 17 (2015) 023011.

[42] J. Durnin, J. J. Miceli, Jr., and J. H. Eberly, "Diffraction-free beams", Phys. Rev. Lett. 58, 1499-1501(1987).

[43] F. M. Dickey and S.C. Holswade (eds.), Laser beam shaping, theory and techniques (Marcel Dekker, New York, 2000).

[44] P. P. J. Zupancic, Dynamic holography and beam shaping using digital micro-mirror devices, Ludwig-Maximilians-Universitat Muchen, Masters Thesis, 2013.

[45] A. Dudley, Superposition of Light fields carrying orbital angular momentum,PhD Thesis, University of KwaZulu-Natal,Duban, 2012.

[46] O. Brzobohaty, V. Karasck, M. Siler, L. Chvatal, T.Cizmar, and P. /zemanek, "Experimental demonstration of optical transport, sorting and self-arrangement using a tractor beam", Nat Photon, Vol. 7, pp. 123-127,2013.

[47] J. Arlt, K. Dholakia, Generation of high order Bessel beams by use of an axicon, Optics Communication 177 (2000) 297- 301.

[48] N. Chattrapiban, E. A. Rogers, D. Cofield, W. T. Hill, III, and R. Roy, Generation of non-diffracting Bessel beams by use of a spatial light modulator, Optics letters, Vol. 28, Issue 22, pp. 2183-2185 (2003).

[49] B. E. A. Saleh, M. C. Teich, Fundamentals of Photonics, John Wiley and Sons, Inc, 1991.

[50] B. Carlos Gonzalez Gomez, Laser Beam Shaping, MSc. Thesis, Brno University of Technology, 2012.

[51] Gaussian beam optics, Available online, accessed at: $www.newport.com/store/product.aspx?id = 144899lang = 1033$

[52] M. Duocastella and C. B. Arnold, Bessel and annular beams for materials processing, Laser Photonics Rev. 6, No. 5, 607–621 (2012).

3 Holographic Beam Shaping

Laser beams form a family of Gaussian beams which are also solutions to the paraxial wave equation were defined mathematically in the previous chapter. This chapter is dedicated to a discussion on how to produce these beams experimentally by transforming the intensity distribution of a laser beam from the input Gaussian pattern into various shapes using the holographic beam shaping technique. We first introduce the topic and then discuss the tools that enable holographic beam shaping, i.e. holography and a Spatial Light Modulator. Subsequently, the holographic beam shaping technique implementation is described. Thereafter, experimental results are analysed and discussed.

3.1 Introduction

A laser beam shape is defined as the irradiance distribution of the light when it arrives at the plane or material of interest [1]. The most common beam shape is the fundamental (TEM_{00}) Gaussian beam produced by most commercial lasers. Beam shaping can be defined as a process that uses suitable optics to modify or reshape the laser beam's spatial profile into novel beam shapes [1, 2].

Beam shaping is essential in producing other patterns of light because a Gaussian profile is not always well suited for some laser applications [3, 4]. Furthermore; some applications require an extremely well controlled intensity profile to accomplish a task properly. For example, laser surgery and laser material processing applications suffer laser induced damage caused by the difference of the central intensity to that of the edge of a laser beam profile. The peak spot size of a Gaussian beam contains only 86.5 percent of the laser beam power and intensity, while at the boundary only 13 percent of the peak intensity [5]; therefore a uniform intensity distribution is ideal for these applications. In optical tweezing and trapping; micro-particle manipulation is possible using the basic Gaussian profile but the use of novel optical beam shapes widens the field and method of manipulation [6, 7]. Through beam shaping, we can produce light fields that possess orbital angular momentum (OAM) [8], and therefore enhancing the light-matter interaction in macro and nano-photonic materials [9].

This research focused on a beam shaping technique which implements an SLM combined with other optics to convert a Gaussian beam to an arbitrary profile. The SLM is a computer controlled device that employs computer generated holograms to modify the properties of a beam. It has the advantage of giving the user an increased flexibility for changing between beam shapes, and it thus has unlimited potential in many laser applications [10]. In this study, the Gaussian beam was modified to produce Vortex, Laguerre-Gaussian, Bessel beams, superpositions of Laguerre-Gaussian beams and superpositions of Bessel beams. Moreover, the propagation properties of these laser modes were studied, as well as their vortex radius dependence on topological charge.

3.2 Tools for Beam Shaping

The ability to create novel beam shapes is consequential of computer generated holograms coupled with an SLM. They serve as the foundation for holographic beam shaping.

3.2.1 Holography and Digital Holography

The word holography is derived from the Greek words, 'holos' which means 'whole' or 'entire' and 'graphein' which means 'to write' [11, 12]. Holography, invented in 1948 by Dennis Gabor, is the practice of making holograms (also known as phase masks); which are defined as a record of the interference pattern of two coherent fields, a reference field and an object field [12, 13]. A hologram may contain information about the amplitude or the phase of a wave field, or both.

Conventional holography is a traditional method of producing holograms and involves two basic procedures; firstly hologram recording (i.e. photographically recording a light field), and then hologram reconstruction (i.e. reconstructing an object from the recorded light field).

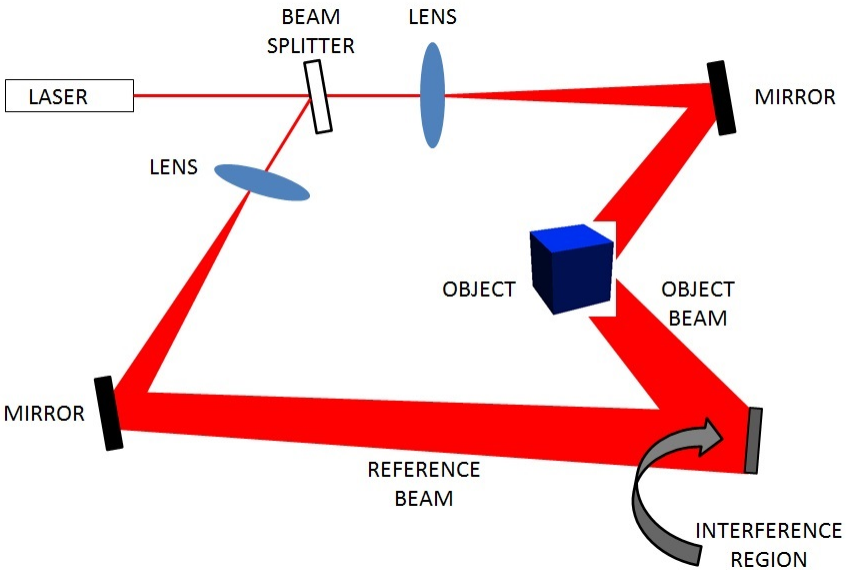

Figure 7: The process of recording a hologram

In a hologram recording process, depicted by Figure 7, the light from a source is split into two beams called the reference beam and the object beam. The object beam is directed onto the object and the object then reflects some light onto the photographic plate (or film). The reference wave reaches the photographic plate unmodified, i.e. still possessing the same properties as the source beam. An interference region is formed in space where these beams interact and the outcome interference pattern is recorded on a high resolution photographic plate. The recorded pattern is termed the hologram.

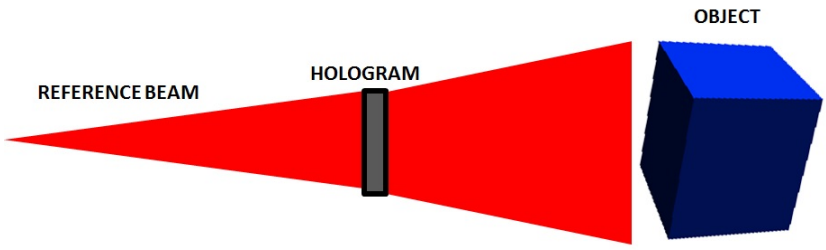

Figure 8: The process of reconstructing an image from a hologram. When a hologram is illuminated with the reference beam, the diffraction pattern recreates the wavefronts of light from the original object, therefore the viewer sees a virtual image of object that is indistinguishable from the real object.

An illustrasion showing the reconstruction of an image from a hologram is represented by Figure 8. This requires illuminating the hologram with a wave possessing the same properties as

the one used to record the hologram. A virtual image is then created and exhibits all the attributes of the original object. It should be noted that the object cannot be identified directly from the hologram, but can only be recognized after the reconstruction process.

3.2.2 Spatial Light Modulator

A spatial Light Modulator (SLM) is a transmissive or reflective device that is used to spatially modulate the amplitude and/or phase of an optical wavefront in two dimensions. An SLM that was used in the research presented in this thesis is a reflective Holoeye Pluto phase-only SLM, shown in Figure 9, which is a system based on a reflective liquid crystal micro-display. It consist of a flex cable, liquid crystal display (LCD) and a circuit board.

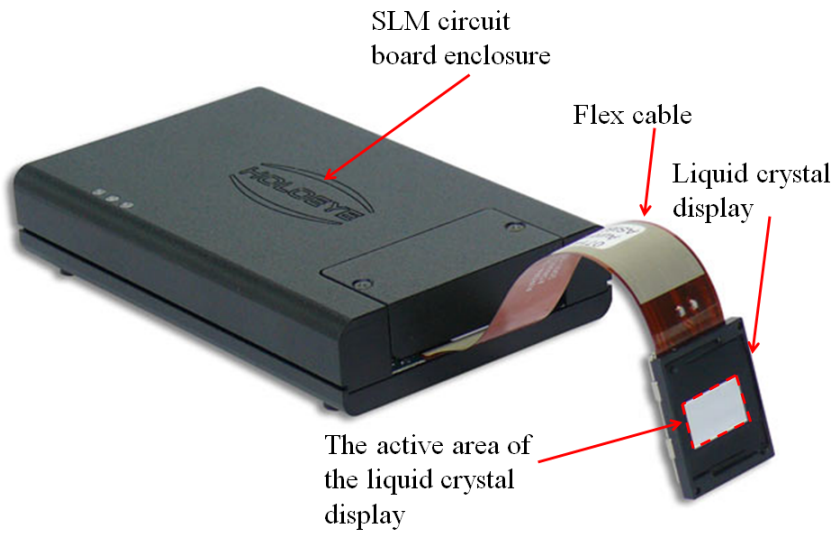

Figure 9: Courtesy of [14]. A Holoeye Phase Only Spatial Light Modulator based on reflective Liquid Crystal on Silicon (LCOS) microdisplay with 1920 x 1080 pixel resolution.

The liquid crystal display (LCD) is the most important element of the SLM; it is programmed and addressed by a circuit board via a flex cable. The circuit board obtains information for controlling the LCD via a conventional interface such as a VGA or DVI input from a computer. The LCD consists of a rectangular grid of 1920×1080 pixels, each having dimension of 8μm, and whose individual transmittance is electronically addressed, i.e., the image is created and changed electronically. The addressing mode of the SLM refers to the type of input signal that controls the optical properties of the SLM. It contains information regarding how the incident light beam should be modified.

The liquid crystal (LC) has both the properties of liquids and crystals. The molecules in the LC are not fixed like those of a crystal, but directionally align themselves almost parallel with each other, and this is a characteristic of crystals.

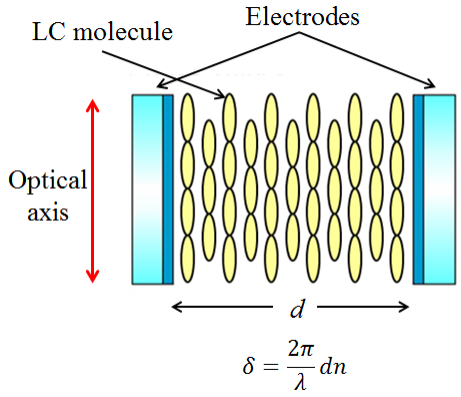

Figure 10: An individual pixel of the liquid crystal display that is addressed by two electrodes separated by a distance d, and modifies the phase of incident light by a phase shift of δ.

Liquid crystals often display unusual and often manipulable optical properties such as anisotropy; consequential of the fact that the LC molecules change orientation when subjected to a force. An individual pixel of the liquid crystal display shown in figure 10, is addressed by two electrodes and the molecules making up the pixel are aligned parallel to the electrodes. When an electric field is applied to the electrodes, the molecules tilt in the direction of the applied electric field. An illustration of this process is given in Figure 10. As the voltage increases the molecules tilt further away from their original position.

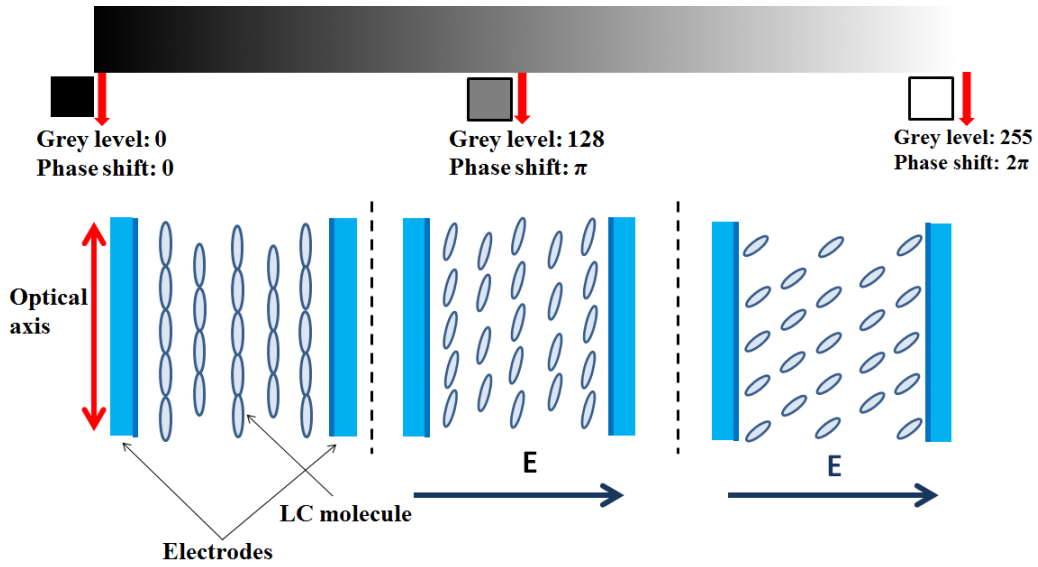

Figure 11: The mechanism of a gray-scale hologram represented on a LCD.

The incident light needs to be linearly polarized, parallel to the axis of the liquid crystal molecules (vertically polarized). When the molecules tilt in the direction of the applied electric field, the refractive index seen by the light changes according to the relationship;

$$\delta = \frac{2\pi}{\lambda} dn, \tag{38}$$

where δ is the phase shift experienced by the beam, λ is the wavelength of the incident light, d is the optical path length in the liquid crystal pixel and n is the refractive index of the liquid crystal pixel, which is proportional to the voltage applied across the electrodes. The light wave propagates with new phase components after being reflected off of one LCD.

The grey scale holograms are represented with 256 grey levels and the voltage across each pixel is adjusted appropriately according to the shade of grey at each pixel in the hologram. Black represents no phase modulation; in this case, no voltage is applied across the electrodes therefore the molecules remain aligned parallel to the electrodes and the LCD acts as a mirror, as depicted by Figure 12 (a). Increasing the voltage applied across the pixels increases the modulation (or grey level). When a grating is encoded on the hologram, the beam is diffracted into many orders, as depicted by Figure 12 (b).

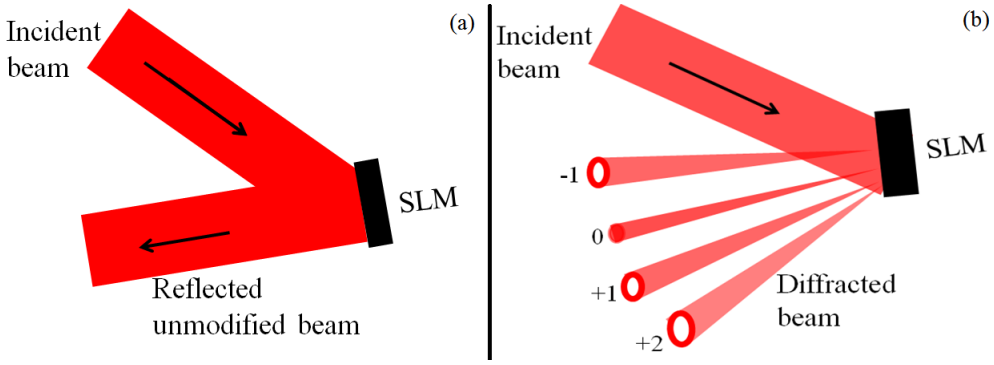

Figure 12: (a) An illustration of the reflection of a laser beam when a black hologram is displayed by the SLM, and in such a case there is no phase shift and the SLM acts as a mirror. (b) An illustration of the diffraction of a laser beam into many orders when a hologram for generating a vortex beam, with a grating, is displayed by the SLM [16].

A grey-scale hologram is computed and programmed into the SLM. The phase of the reference beam is altered according to the phase modulation of the shade of grey present at each pixel of the computer generated hologram.

An SLM can be applied in optical set-ups for beam shaping and with the correct hologram it can be used to realize different optical elements, e.g. it can be used as an axicon, wave plate, gratings, etc., and therefore it can be regarded as a dynamic optical element [17].

3.3 Techniques of Generating Novel Beam Shapes

In this section, we present a few methods which can be used to generate novel beam shapes. There are several methods proven to produce novel beam shapes, ranging from the old traditional to more sophisticated and efficient holography-based methods. Traditional optical elements that control and modify the wave front of light beams depend on the phase introduced while

propagating through the material [18]. The essence of beam shaping is to design an optical system that must operate on the input beam inorder to produce the desired output at the targe plane.

3.3.1 Vortex Beams

A vortex beam arises whenever the beam possess an azimuthal phase structure $exp(il\theta)$. The presence of this azimuthal phase indicates that the phase of the beam changes continuously from 0 to 2π with a round trip on a circle around the azimuthal axis. The integer l is called the topological charge. A traditional method of generating a vortex beam makes use of an optical element called a spiral phase plate (SPP), and was first demonstrated by Beijersbergen et al [20]. A SPP is an optical component with one flat optical surface and a helical optical surface; the thickness of the helical surface increases with azimuthal position. When a Gaussian beam, which has a plane wave phase profile, passes through a SPP, the Gaussian beam accumulates a phase change so that the emerging beam has a spiral phase profile and thus a doughnut shaped pattern, which is demonstrated by Figure 13.

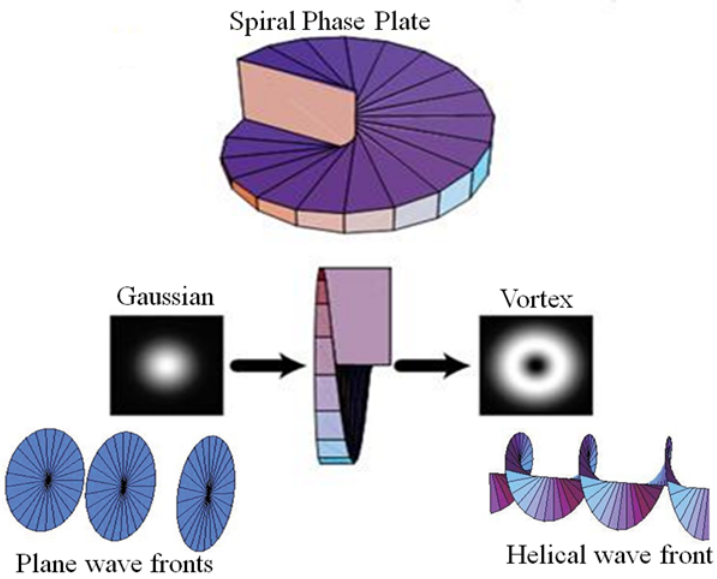

Figure 13: Courtesy of Courtial and O'Holleran,2007 [21]. A Gaussian beam, which has a plane wave front is incident on a SPP and which is converted into a vortex beam possessing a helical wave front.

A recent method of producing vortex beams is by using a computer generated spiral hologram encoded on an SLM. The same concept of helical phase change is used when creating the spiral hologram. A spiral hologram, (shown in Figure 14) is a grey scale image of a helical phase ramp that varies from black to white corresponding to phase change from 0 to 2π. When a grating is embedded on a spiral hologram, a fork hologram is produced, also shown in Figure 14. When shining a laser emitting the fundamental TEM_{00} mode onto the SLM encoded with a fork hologram, the beams phase is modified in the same way as with a SPP.

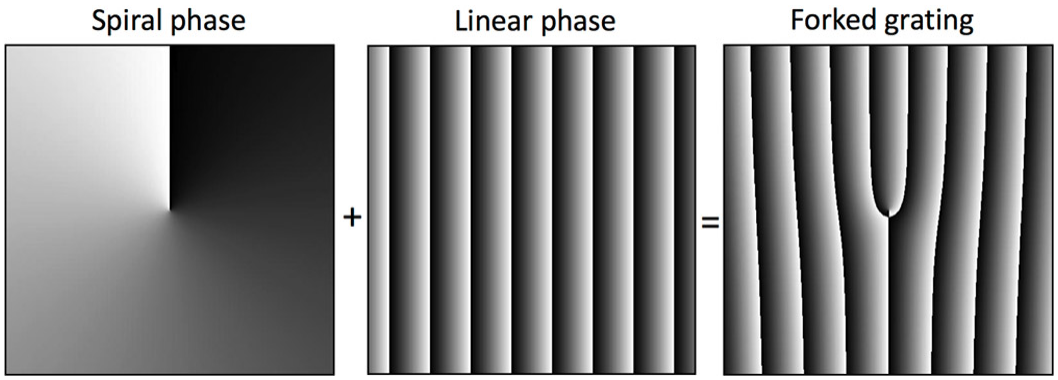

Figure 14: Courtesy of Moreno and Davis, 2013 [22]. Combining a spiral phase pattern with the phase of a linear blazed grating results in a forked grating.

3.3.2 Bessel Beams

The first experimental realization of a Bessel beam (non-diffracting beam-NDB) was performed by Durnin et.al. [19], in 1987, and was achieved using an annular aperture and a lens, a schematic of this approach is given in Figure 15. This method involves placing an annular aperture at the back focal plane of a lens and illuminating it with a Gaussian beam. This produces conical wave fronts after the lens which interfere to produce a Bessel beam. This approach is inefficient because the aperture blocks most of the incident beam.

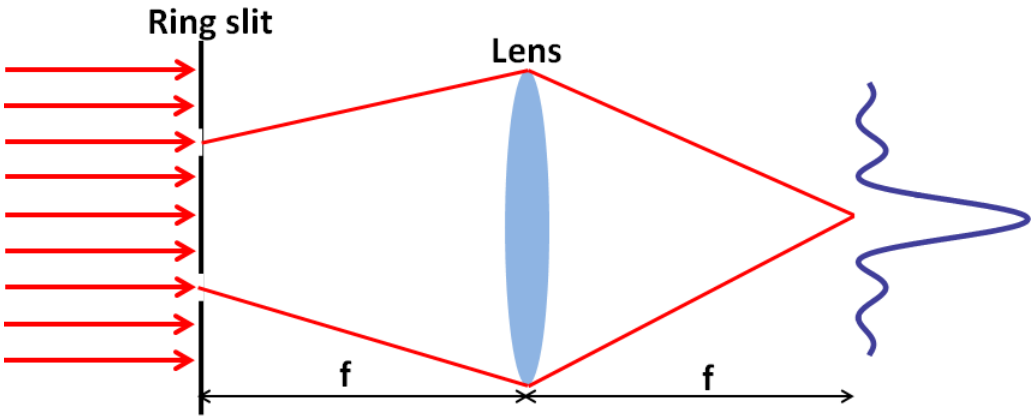

Figure 15: An annular aperture placed at the back focal plane of a lens is illuminated with a Gaussian beam to produce a Bessel beam.

Another method of generating a Bessel beam is by using an axicon [23], also called a conical lens. In this case, conical wave fronts are generated after the axicon when a Gaussian beam is incident on it, and the wave fronts interfere producing a Bessel beam, as shown by Figure 16.The axicon has been widely used to generate NDBs and HOBBs with high conversion efficiencies close to 100 [23, 24]. This method is more efficient than the aperture based method, but its disadvantage is that the alignment between the incident beam and the axicon is crucial and can result in a non-uniform output beam if not correctly aligned.

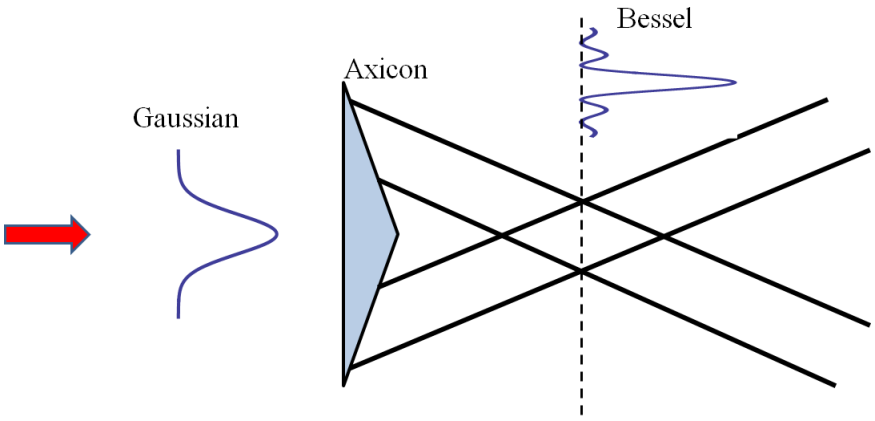

Figure 16: The construction of a Bessel beam by an axicon requires illuminating an axicon with a Gaussian beam.

The SLM based method is the most commonly used method of generating Bessel beams nowadays. In this case, mathematical methods are used to generate an axicon type or the ring-slit type CGHs that modifies the incident beam in the same way as an axicon or the ring-slit, respectively. The hologram is then uploaded onto the LCD of the SLM, and when illuminated with a Gaussian beam produces a Bessel beam. The hologram is produced dynamically; therefore it is easy to modify the properties of the Bessel beam produced.

An SLM that can control both amplitude and phase is needed for the generation of a ring slit phase mask. The region within a ring slit modifies the phase of the incident beam. For a phase only SLM, like the one used in our experiments, the sections of the phase mask in which we do not want to transmit any light are encoded with a checkerboard pattern. The checkerboard pattern consists of a grid of alternating black and grey pixels [25].

Bessel beams have found a variety of applications especially in optical trapping [26]. For instance, the ring structure of Bessel beams makes it possible to simultaneously trap both low and high index particles [27], while thir self-reconstruction property has enabled the simultaneous trapping of particles that are spatially separated [28]. The trapped micro-particles have been shown to rotate owing to the transfer of OAM and spin angular momentum (SAM), and their rotation has been measured [27].

3.4 Experimental Set-up and Methodology

We describe an experimental technique to generate laser modes with intensity distributions described by equations (32), (34) and (37), and the coherent superposition of each of the two latter modes (i.e. LG and BG). The experimental set-up for the realization of holographic beam shaping is shown in Figure 17. In the set-up, a HeNe laser of 632.8 nm is expanded by a 5 $\times$ telescope made with lenses f_1 and f_2 so as to cover the SLM's entire active area.

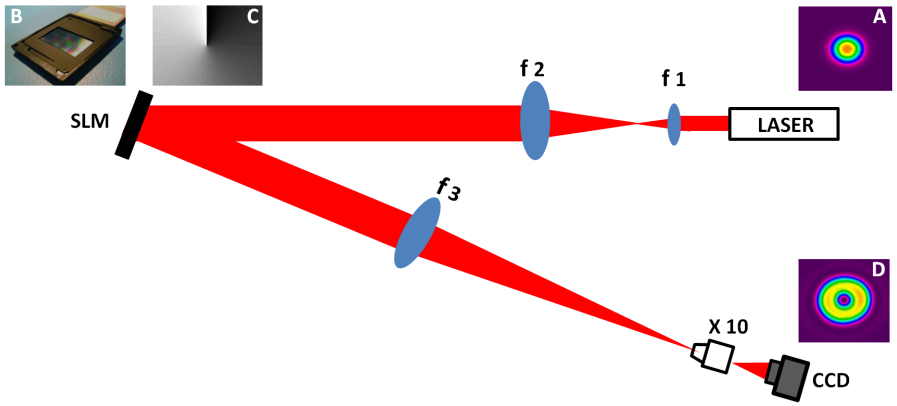

Figure 17: The experimental set-up used for the realization of laser beam shaping with the SLM.

An expanded Gaussian beam profile then propagates to the SLM where it is modulated by a computer generated hologram uploaded onto the SLM. The resulting field distribution is maintained along the progagation path. Furthermore, the beam reflection from the SLM is diffracted into many orders, and whence a pinhole performs spatial filtering by selecting only the first diffraction order. Spatial filtering is essential to minimize the overlap and interference effect of different diffraction orders of the output intensity distribution at the plane of the camera.

Subsequently, the beam passes through the Fourier transforming lens f3 of focal length 500 mm, and at the focal plane expanded by a 10 × objective lens so that the resulting intensity distribution is captured by a CCD camera which is connected to a computer. A combination of filters were used to control and reduce the amount of laser radiation incident on the camera so as to prevent laser induced damage on the CCD.

Various beam profiles were generated, and suitable manipulations made for the realization of different experimental investigations. A camera together with its beam profiling software gave the visualization of the resulting beam profile, which was then captured for analysis.

3.5 Results and Discussion

Holographic beam shaping enables the manipulation of the incident laser profile as well as the generation of novel beam shapes. A wide range of possiblities provided by the SLM were explored. All the experimental results presented in this section and shown in the figures constitute a representative example of successful execution of holographic beam shaping. The modifications of the beam profile and experimental investigations accomplished in this study are presented in the following subsections.

3.5.1 Experimental Generation of Laser Mode Patterns

A study of the various far field intensity patterns produced in the camera plane was conducted. Optical vortex beams produced experimentally (dots) and theoretically (solid line) are depicted by figure 18 (a). An optical vortex was obtained by imposing a helical phase hologram, Figure 18 (b), onto the input beam by utilising an SLM, then a vortex beam was generated upon reflection from the SLM. A pinhole was used to select the first order, and then imaged to the camera plane. The transverse mode structure of the output beam, depicted by figure 18 (c), was captured by a CCD camera in a plane perpendicular to the propagation axis of the beam, and the corresponding

theoretical intensity profile, depicted by figure 18 (d), was generated in Mathematica.

The experimental and theoretical pictures have colours ranging from red to purple, corresponding to intensity variation from highest to lowest. Numerical values of the intensity at the Fourier plane were found by saving the image as an ascii file. In Mathematica, intensity was plotted as a function of radial distance along with the theoretical mode intensity profile, depicted in figure 18 (a). The parameters of the theoretically generated beam were defined such that they suit those of the experiment. This procedure was followed with the other intensity distributions generated, the only difference being the hologram encoded on the SLM.

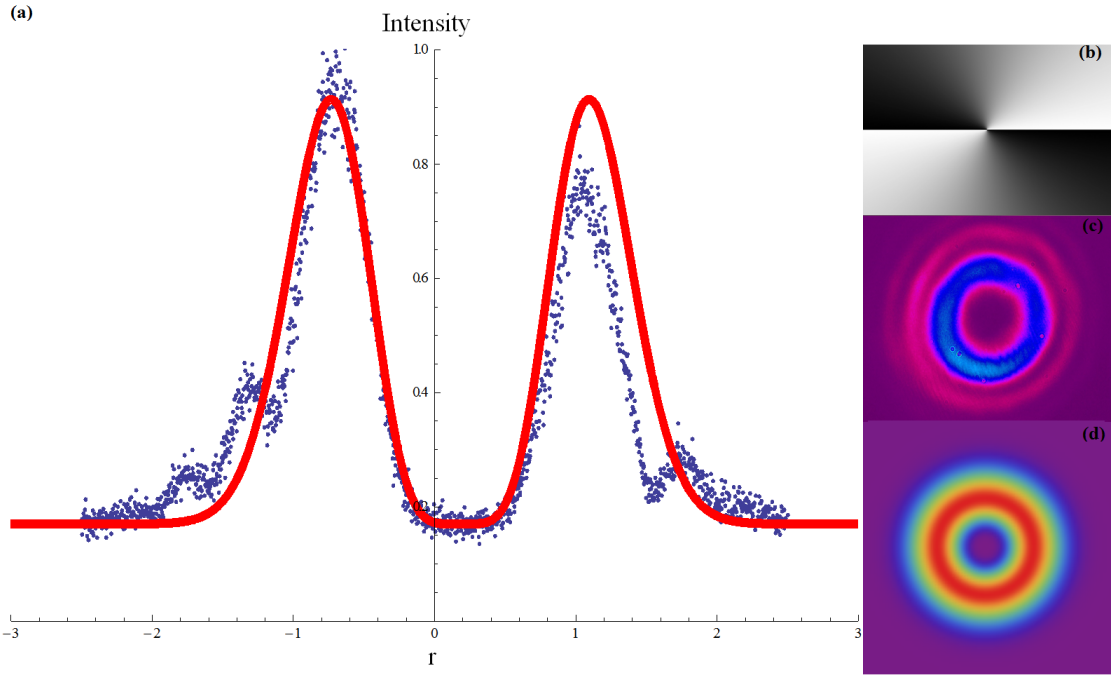

Figure 18: The experimental (dots and (c)) and theoretical (solid line and (d)) profiles of a vortex mode of topological charge $l = 2$ together with (b)the phase hologram used to produde the vortex beam.

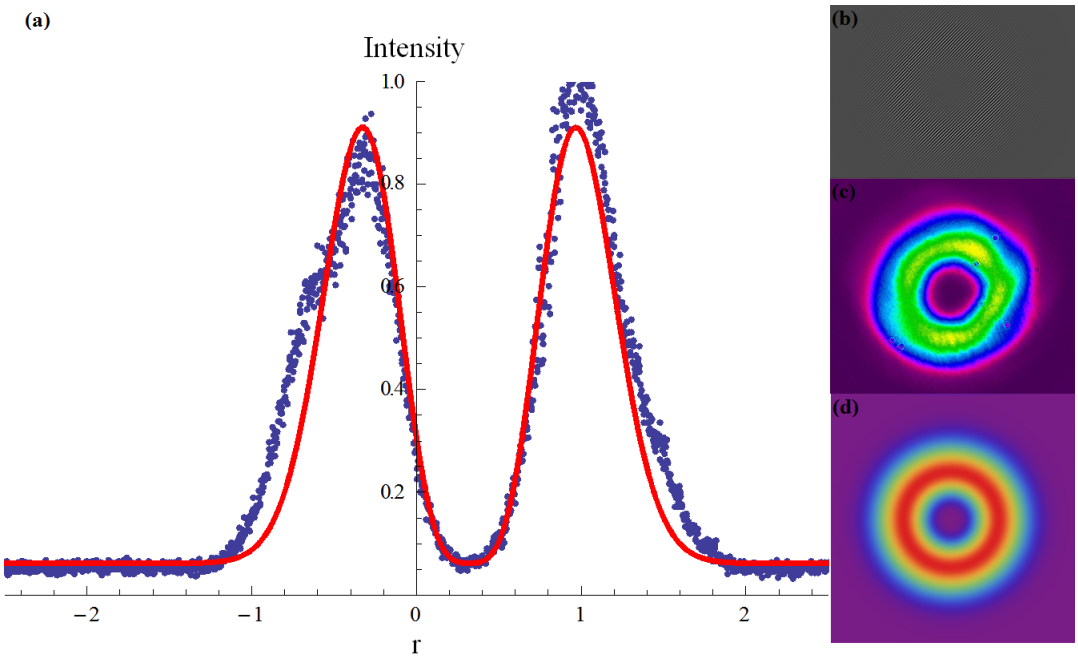

Figure 19: The experimental (dots and (c)) and theoretical (solid line and (d)) profiles of a Laguerre-Gaussian mode of topological charge $l = 2$ produced depicted together with the phase hologram (b) used to produde the LG beam.

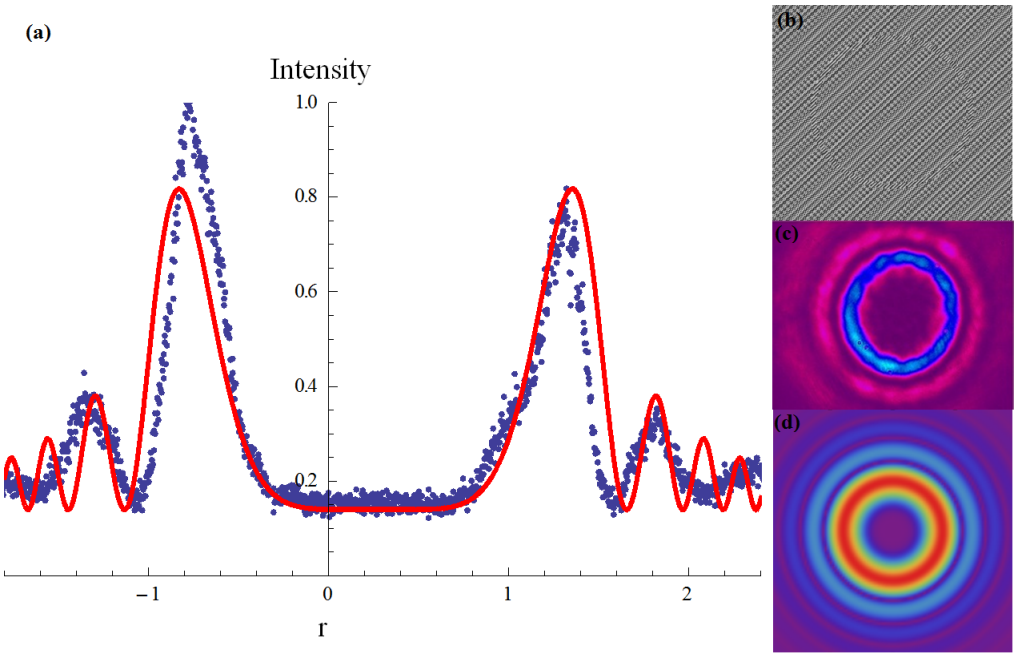

Figure 20: The experimental(dots and (c)) and theoretical (solid line and (d)) profiles of a Bessel-Gauss mode of topological charge $l = 7$ depicted together with the phase hologram (b) used to produde the Bessel beam.

Similary, experimental and theoretical profiles of Laguerre-Gauss and Bessel Gauss beam were produced as depicted by Figure 19 and Figure 20, respectively. It is evident that the characteristic shape of theoretical and experimental laser beams are in agreement.

Laser modes can be superimposed onto one another to generate higher order modes, and higher order modes are characterised by a far field pattern that, in some cases, consist of petals. For each of the original modes superimposed, the light fields transverse profile is a continuous circular pattern, however for the superposition modes, lines of discontinuity exist and thus changing the pattern to posses petals. For modes with identical azimuthal mode indices, the number of petals in the pattern was found to be $2 \times l$ (topological charge value) of the superimposed modes. Two mode superpositions of same azimuthal order Bessel beams were experimentally generated, depicted by Figure 21 together with the corresponding ring slit holograms.

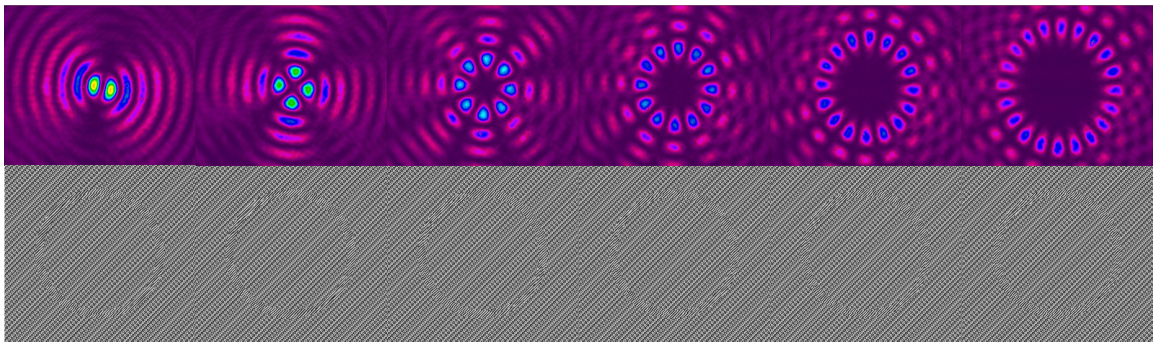

Figure 21: Two mode superpositions of azimuthally same order Bessel beams of topological charge 1, 2, 4, 6, 8 and 10, together with ring-slit holograms that were used to produce the modes.

3.5.2 Propagation of Superimposed Bessel-Gauss Modes

Holo_SP_BG1.png

Figure 22: A phase hologram with a ring slit aperture with radius R and width 2Δ for producing superposition of $l = 4$ and $l = -4$ Bessel beams together with the far field intensity distribution.

The incident Gaussian beam was projected onto an SLM, where an azimuthally varying phase was transmitted to the angular spectrum of the beam [29]:

$$\Phi(r,\varphi) = \begin{cases} exp(im\varphi) \\ exp(in\varphi) \end{cases} \tag{39}$$

This angular spectrum is then transformed into a superposition of two Bessel beams of order m and n by a Fourier transforming lens. The resulting superposition is calculated numerically by the use of the Kirchoff-Huygens diffraction integral [29, 30]:

$$A_{m,n}(r,\phi,z) = \frac{-i}{\lambda z}\int_0^{2*\pi}\int_{R-\Delta}^{R+\Delta}\tau(r,\phi)exp\left[i\frac{k_0}{2f}\left(1-\frac{z}{f}\right)r_1^2\right]exp\left[i\frac{k_0 r r_1}{f}cos\left(\phi_1-\phi\right)\right]r_1 dr_1 d\phi_1, \tag{40}$$

and may be represented in the form [29]:

$$A_{m,n}(r,\phi,z) = A_m(r,\phi,z) + A_n(r,\phi,z), \tag{41}$$

where

$$A_m(r,\phi,z) = \frac{-ik_0 i^m}{f}exp(im\varphi)\int_{R-\Delta}^{R} exp\left[-\frac{r_1^2}{w^2}+\frac{ik_0 r_1^2}{2f}\left(1-\frac{z}{f}\right)\right]J_m\left(\frac{k_0 r r_1}{f}\right)r_1 dr_1, \tag{42}$$

and

$$A_n(r,\phi,z) = \frac{-ik_0 i^n}{f}exp(in\varphi)\int_{R-\Delta}^{R} exp\left[-\frac{r_1^2}{w^2}+\frac{ik_0 r_1^2}{2f}\left(1-\frac{z}{f}\right)\right]J_n\left(\frac{k_0 r r_1}{f}\right)r_1 dr_1. \tag{43}$$

Apart from investigating the field produced at the Fourier plane, the propagation of these fields was also investigated. It was noted that the intensity profile of the field rotates during the beams propagation. When moving the CCD camera along the propagation axis (z) over some distance z, the lobes rotate by an angle θ.

In order to verify quantitatively this variation, the rotation angle was measured along the z-axis with a moving CCD-camera. In the measurement, the focal length of the Fourier transforming lens is given as $z = 0$mm and at this position the angle rotation of the image is 0 degrees. For all other distances $z > 0$ mm, the CCD camera captured the intensity profile and thus rotation of the petals in steps of $\Delta z = 20$ mm from the chosen origin. The intensity distributions produced are depicted by Figure 23, and are circular and symmetric with 8 petals.

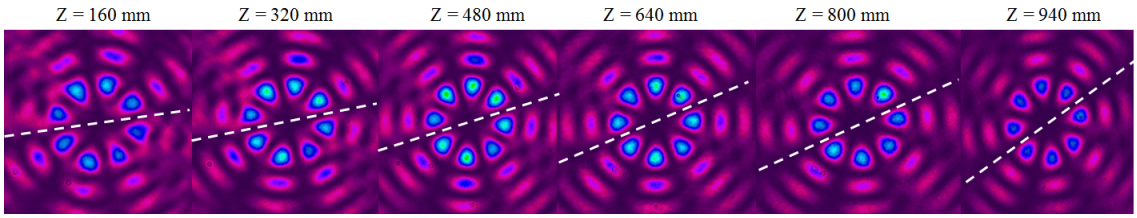

Figure 23: The intensity profile for the superposed Bessel beams propagated and captued at different planes along the propagation axis. The dashed line illustrates the angular rotation of petals during propagation.

The experimental propagation of superposed modes is associated with on-axis rotation of the petals. This rotation was measured as a function of propagation distance, depicted by Figure 24. The linear rotation of a Bessel beam with propagation distance provides evidence that Bessel beams indeed do possess OAM. The rotating fields are an ideal tool for producing controlled rotation of trapped particles in optical trapping experiments [31].

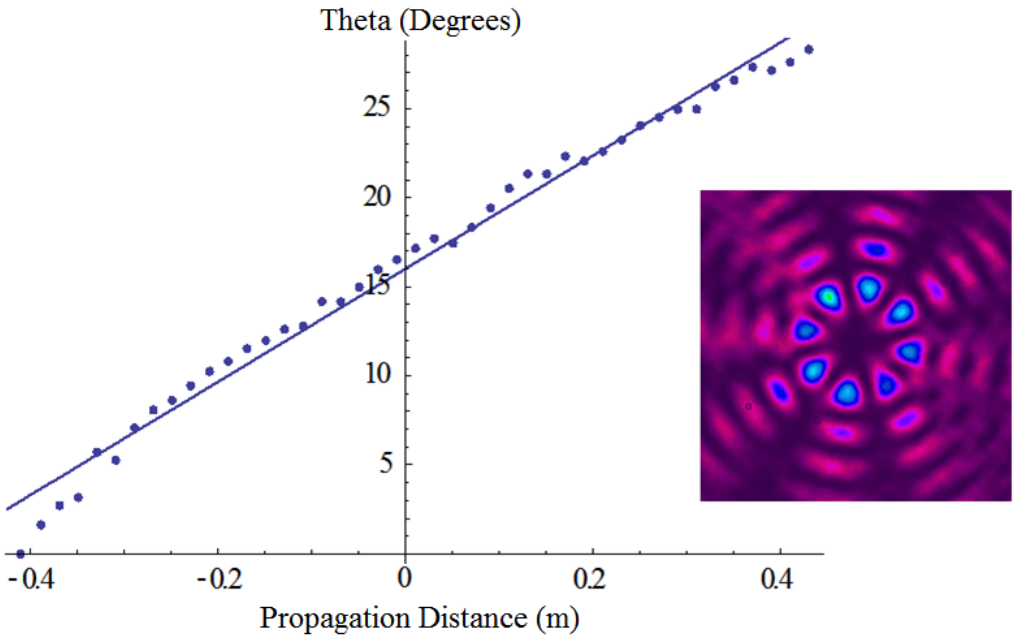

Figure 24: The measured rotation Theta (Degrees) of the petals plotted against propagation distance.

3.5.3 Beam Radius Dependence on Topological Charge

Experimental investigation of vortex radius dependence on topological charge for vortex, LG and Bessel beams was realized by uploading holograms with various topological charge values onto the SLM and then capturing the far field intensity profile at the plane of the camera. The vortex diameter was measured for each captured profile, and then subsequently plotted in Mathematica.

The theoretical equation that describes vortex radius dependence on topological charge for the Laguerre-Gauss beam which possesses a radial index $p = 0$ is given by equation 35. This equation is also applicable for vortex beams since the vortex beam is the LG beam with radial index, $p = 0$. The theoretical equation describing the dependence of the Bessel vortex radius on topological charge is not readily available, and was obtained by first finding the Bessel vortex radius by solving the Bessel intensity profile, given by equation 37, for the position of the first null intensity, and subsequently plotting the vortex radius versus the azimuthal index l.

The resulting profiles of vortex radius dependence on topological charge are given by Figures 25-27 where the experimental results (blues dots) were fitted with the theory (red line).

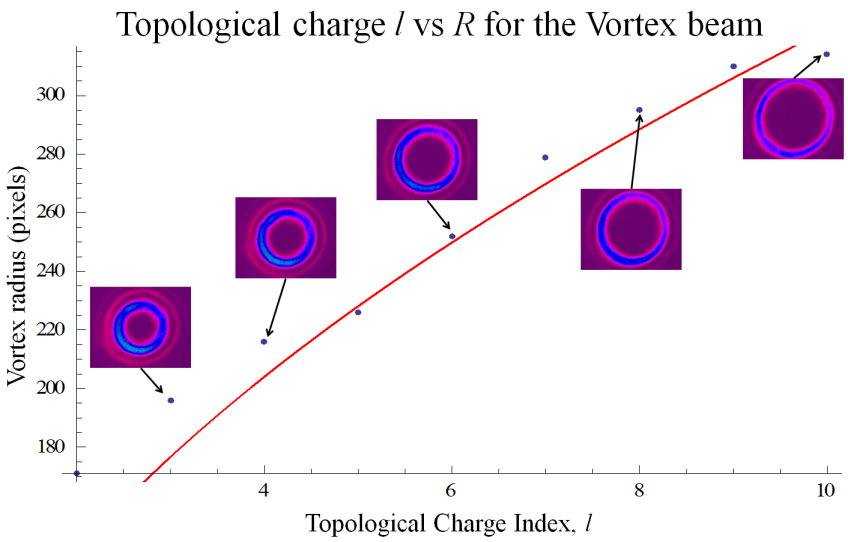

Figure 25: The vortex beam radius dependence on topological charge.

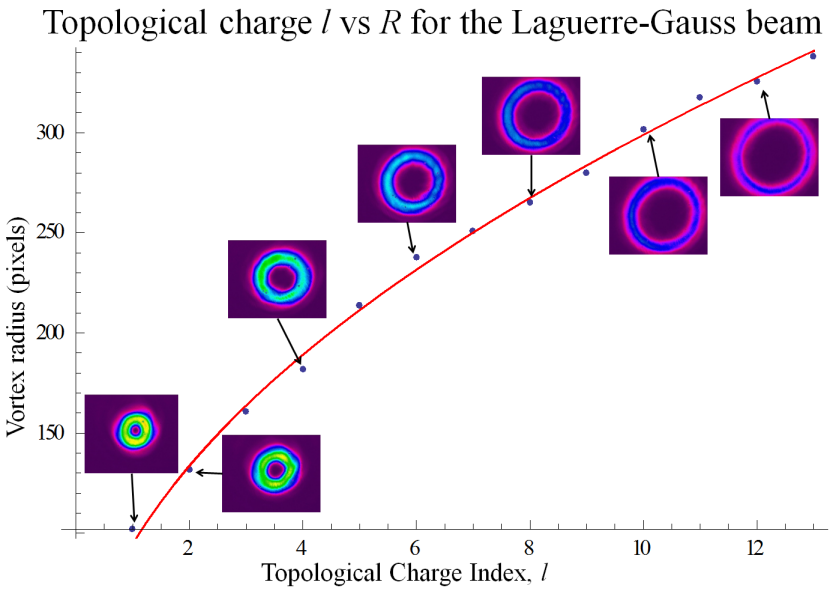

Figure 26: The Laguerre-Gauss beam radius dependence on topological charge for the beam with radial index $p = 0$.

It is evident that the experimental results are in agreement with the theory; they show that the vortex radius increases with the azimuthal index for all three types of beams investigated.

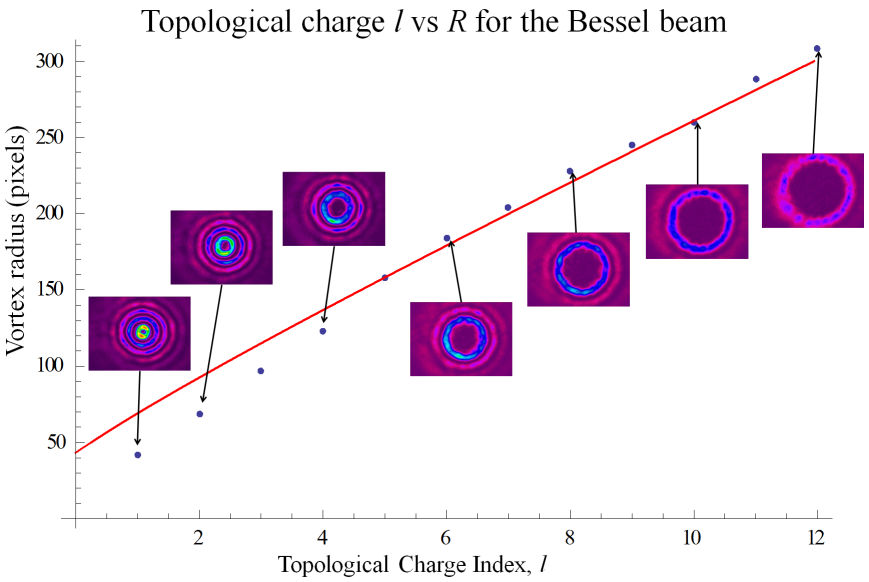

Figure 27: The Bessel beam radius dependence on topological charge.

3.6 Summary

A historical review of holography and the subsequent development of digital holography was presented. Holographic beam shaping technology creates new laser capabilities and optimizes a number of applications. We have achieved laser beam shaping by employing a holographic technique, which is a more efficient design of producing different laser modes. A programmable LC-SLM was used to manipulate and transform a Gaussian beam profile into vortex, Bessel, Laguerre-Gauss beam or superposition modes. Experimental and theoretical studies on the properties and dynamics of these beams have been presented. Methods for measuring their transverse properties were discussed, each profile produced experimentally matched the theoretically generated profile. Superimposed Bessel-Gauss irradiance distributions have been produced to investigate their propagation dynamics. It was found that the propagation of superposition modes is accompanied by on axis rotation of the intensity profile. Finally beam radius dependence on topological charge was investigated, and for all beams investigated the beam radius increased with topological charge index. Holographic techniques are very efficient in that they can be easily adapted to a variety of applications.

References

[1] F. M. Dickey and S.C. Holswade (eds.), Laser beam shaping, Theory and Techniques (Marcel Dekker, New York, NY, 2000)

[2] F. M. Dickey, L. S. Wiechman and R. N. Shangan, Laser Beam Shaping Techniques, Accessed at: http://www.osti.gov/scitech/servlets/purl/752659/

[3] Gaussian Versus Flat-top Beam Processing, Accessed online; at: $http://www.spectra-physics.com/assets/clientfiles/files/documents/Flat-topLaserSolarScribingSP.pdf$

[4] M. Duocastella and C. B. Arnold, Bessel and Annular Beams for Materials Processing, Laser Photonics Rev. 6, No. 5, 607–621 (2012).

[5] G. Raciukaitis, E. Stankevicius, P. Gecys, M. Gedvilas, C. Bischoff, E. Jager, U. Umhofer and F. Volklein, Laser Processing by Using Diffractive Optical Beam Shaping Technique, JLMN-Journal of laser Micro/Nanoenginnering, Vol. 6, No. 1, 2011.

[6] K. Dholakia, G. Spalding and M. MacDonald, Optical tweezers: The Next Generation, Physics World, October 2002. Accessed at $www.colorado.edu/physics/phys2170/phys2170_sp07/downloads/PWOCT02optical - tweezers$.

[7] B. K. Singh, H. Nagar, Y. Roichman, and A. Arie, Particle Manipulation Beyond the Diffraction Limit Using Structured Superoscillating Light Beams, Accessed online: $https : //arxiv.org/ftp/arxiv/papers/1609/1609.08858.pdf$

[8] M. Mirhosseini, O. S. Magana-Loaiza, C. Chen, B. Rodenburg, M. Malik, and R. W. Boyd, Rapid Generation of Light Beams Carrying Orbital Angular Momentum, Optical Society of America, Vol. 21, No. 5, 2013.

[9] K. Sakai, T. Yamamoto and K. Sasaki, Nanofocusing of Structured Light for Quadrupolar Light-Matter Interactions, Scientific Reports, Vol. 8, 7746 (2018).

[10] A. J. Turska, B. Atamaniuk and E. Turska, Fractional Derivative Analysis of Helmholtz and Paraxial-Wave Equations, Department of Theory of Continuos Mechanics, Institute of Fundamental Technological Research, PAS, 2002.

[11] F. F. Mazda, Discrete Electronic Components, Cambridge University Press, United States of America, 1981.

[12] U. Schnars, W. Jueptner, Digital holography: Digital hologram recording, Numerical Reconstruction, and Related Techniques, Springer-Verlag Berlin Heidelberg, Germany, 2005.

[13] D. Meschede, M. Fiebig, quantum-technologies.iap.uni-bonn.de/de/diplom-theses.html?task

[14] PLUTO Phase Only Spatial Light Modulator (Reflective) [Online]. Available at: http://holoeye.com/spatial-light-modulators/slm-pluto-phase-only/

[15] G. A. Cirino, P. Verlonck, R. D. Mansano, J. C. Pizolato Jr., D. B. Mazulquim and L. G. Neto, Digital Holography: Computer Generated Holograms and Diffractive Optics in Scalar Diffraction Domain, accessed online at: cdn.intechopen.com/pdfs-wn/19622.pdf.

[16] J. E. Morris, (2010). Studies of Novel Beam Shapes and Applications to Optical Manipulation, PhD Thesis, University of St. Andrews. Accessed from: https://research-repository.st-andrews.ac.uk/handle/10023/1699

[17] A. Bamberger, B. Engquist, L. Halpern and P. Joly, Higher Order Paraxial Wave Equation Approximations in Heterogeneous Media, SIAM Journal of Applied Mathematics (1998),Pages 129-154.

[18] M. Born and E. Wolf, Principles of Optics, 7th ed. (Cambridge University Press, Cambridge, 1999).

[19] J. Durnin, J. J. Miceli, and J. H. Eberly, Diffraction-Free Beams, Phys. Rev. Lett. 58, 1499 (1987).

[20] M. W. Beijersbergen, L. Allen, H. E. L. O. van der Veen and J. P. Woerdman, "Astigmatic Laser Mode Converters and Transfer of Orbital Angular Momentum," Opt. Commun. 96, 123-132 (1993).

[21] J. Courtial and K. O'Holleran, Experiments with twisted light: Some of the Mechanical and Quantum-Mechanical Properties of Optical Vortices, Eur. Phys. J. Special Topics 145, 35-47 (2007).

[22] Ignacio Moreno and Jeffrey A. Davis, Controlling Vortex Light Beams, accessed at: http://spie.org/newsroom/4965-controlling-vortex-light-beams

[23] R. M. Herman, T. A. Wiggins, "Production and uses of diffractionless beams," J. Opt. Soc. Am. A 8, 932-942 (1991)

[24] V.S. Ilchenko, M. Mohageg, A. A. Savchenkov, A. B. Matsko, and L.Maleki, "Efficient Generation of Truncated Bessel Beams Using Cylindrical Waveguides", Opt. Express, Vol. 15, No. 9, 5866-5871 (2007).

[25] A. Dudley, R. Vasilyeu, V. Belyi, N. Khilo, P. Ropat, and A. Forbes, Controlling the Evolution of Non-Diffracting Specle by Complex Aamplitude Modulation on a Phase-Only Spatial Light Modulator, Optics Comm., 285 (2015), 5-12.

[26] G. S. Sokolovskii, V. V. Dudelev, S. N. Losev, K. K. Soboleva, A. G. Deryagin, V. I. Kuchinskii, W. Sibbett and E. U. Rafailov, "Optical Trapping with Bessel Beams Generated from Semiconductor Lasers", J. Phys.: Conf. Ser. 572 012039 (2014).

[27] V. Garces-Chavez, K. Volke-Sepulveda, S. Chavez-Cerda, W. Sibbett, and K. Dholakia, "Transfer of Orbital Angular Momentum to an Optically Trapped Low-Index Particle", Phys. Rev. A, vol. 66, 063402, 2002.

[28] V. Garces-Chavez, D. McGloin, H. Melville, W. Sibbett, and K. Dholakia, "Simultaneous Micromanipulation in Multiple Planes Using a Self-Reconstructing Light Beam", Nature, vol. 419, p. 145, 2002.

[29] R. Vasilyeu, A. Dudley, N. Khilo and Andrew Forbes, "Generating Superpositions of Higher–Order Bessel Beams", Opt. Express, 17(26), 23389-23395 (2009).

[30] R. Rop, A. Dudley, C. Lopez-Mariscal and A. Forbes, Measuring the rotation rates of superpositions od higher –order Bessel beams, Journal of Modern Optics, Vol. 59, N0. 3, 2012(259-267).

[31] S. N. Khonina, V. V. Kotlyar, R. V. Skidanov, V. A.Soifer, K. Jefimovs, J. Simonen and J. Turunen, Rotation of Microparticles with Bessel Beams Generated by Diffractive Elements,Journal of Modern Optics, Vol. 51, No. 14, (2004)2167-2184.

[32] H.G. Heard, Laser Parameter Measurement Hand Book, John Wiley and Sons, Inc., USA, New York, 1968.

[33] G. Laufer, Introduction to Optics and Lasers in Engineering, Cambridge University Press, USA, New York, 1996

[34] D. McGloin, K. Dholakia,Bessel beams: Diffraction in a New Light, Contemp. Phys. 2005,46,15-18.

[35] L. Allen, M. W. Beijersbergen, R. J. C. Spreeuw, and J. P. Woerdman, "Orbital angular momentum of light and the transformation of Laguerre-Gauss modes," Phys. Rev. A 92, 8185–8189 (1992)

4 Generation of Off-Axis Vortex Beams

A pure vortex beam is produced when a Gaussian beam is incident on a spiral phase mask on axis. If the propagation axis of the input Gaussian beam does not coincide with that of the phase hologram, the resulting beam is a superposition of vortex and Gaussian modes (also called an off-axis vortex). A method of creating off-axis vortex beams is presented, and the far field features of such beams were studied. Small off-axis displacements produce a far field pattern that is an asymmetric vortex beam with its singularity point displaced off-axis. It was observed that the vortex structure appears and disappears as the displacement of the hologram singularity is varied. The degree of asymmetry of the superposition beam was found to depend on the magnitude of the singularity displacement from the origin. The experimental observations were in good agreement with the expected results, and with the results reported by other researchers.

4.1 Introduction

Optical vortices have drawn so much interest because of their unusual characteristics as well as possible application in the manipulation of trapped micro-particles [1]- [3]. The characteristics of an off-axis vortex beam differ from that of an on-axis vortex beam. An observable difference is the physical structure; a vortex beams possesses a phase singularity at the centre, while for an off-axis vortex mode the singularity is shifted from the beams axis. An off axis vortex is also characterized by an asymmetric transverse intensity profile with unequal peak values such that one peak is bigger than the other, also depicted by Figure 28. The degree of asymmetry of an off-axis vortex beam depends on the displacement of the singularity point from the origin, reported by Anzolin et. al (2009) [5].

Figure 28 was computed in Mathematica, and shows a simulation of the evolution of a vortex beam from an on-axis vortex to an off-axis vortex and then to a Gaussian intensity profile; this is related to the displacement of the hologram with respect to the input Gaussian beam.

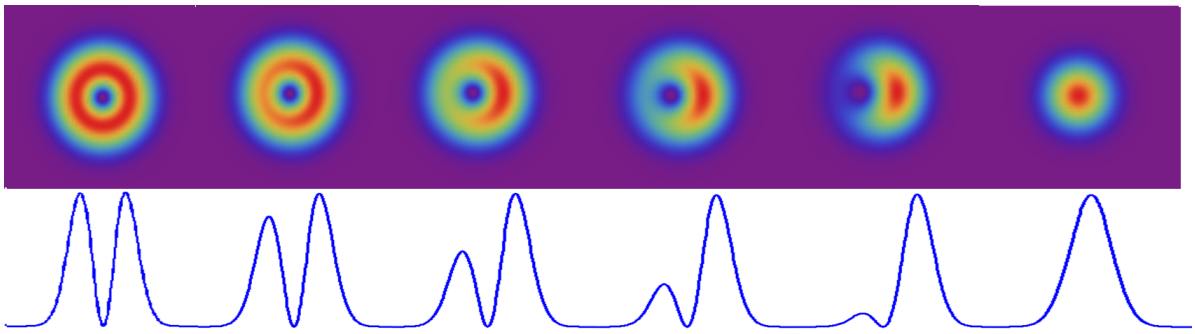

Figure 28: The evolution of a vortex beam from an on-axis vortex to off-axis: When the axis of the input Gaussian mode coincides with that of the spiral hologram, a pure Vortex is produced. When the hologram is displaced off-axis (e.g. along the x-axis), the output beam is an off-axis vortex and the degree of asymmetry of an off-axis vortex depends on the magnitude of singularity displacement from the centre. The vortex mode decreases from left to right, while the Gaussian mode increases from left to right.

Optical vortices are light beams with an azimuthal phase structure $exp(il\phi)$, where l is an integer number, and carry OAM of $l\hbar$ per photon [16]. On the contrary, off-axis beams possess a

non-integer topological charge value, and thus carry fractional OAM [7].

In this section, we present a method to experimentally produce and study the behaviour of a beam that is a coherent superposition of Gaussian and vortex modes. The analytic expressions for the field distribution of an off axis vortex beam is presented. The experiment is performed by using an SLM encoded with various holograms possessing shifted singularity points. We show that off-axis displacements of the spiral hologram with respect to the input beam produces an asymmetric vortex beam, and that the degree of asymmetry of an off-axis vortex beam depends on the displacement of the singularity point from the origin.

4.2 Theory

A field U, that is a coherent superposition of vortex and Gaussian modes has an analytical expression given by:

$$\begin{aligned} U(r,x,y,z) &= \alpha Gaussian + \beta Vortex \\ &= \alpha\Big[exp\Big(\frac{-r^2}{\omega(z)^2}\Big)\Big] + \beta\Big[(x+iy)\times exp\Big(\frac{-r^2}{\omega(z)^2}\Big)\Big], \end{aligned} \tag{44}$$

where α and β are the weighting coefficients of the Gaussian and vortex modes, respectively. All other parameters have the same definition as in the previous chapters. The weighting coefficients give a measure of each mode present in the mixed mode U, and a certain pair of weightings yields a unique intensity profile. A few selections were chosen and then numerically generated using Mathematica to show the vortex's evolution from pure vortex to pure Gaussian mode, depicted by Figure 28. It is evident that the vortex structure appear and disappear as the displacement of the hologram singularity from the origin is increased.

4.3 Experimental Set-up and Methodology

An experimental set-up for generation of off-axis vortex beams is presented in Figure 29. A He -Ne laser beam of wavelength 632.8 nm was directed towards the SLM (a holoeye, pluto phase only reflective SLM). When the SLM was encoded with a phase mask that posessed an on-axis singularity point, a pure symmetric vortex was produced. Generating a field that is a coherent superposition of vortex and Gaussian modes was achieved by generating phase masks with a shifted singularity point. A beam profile reflected from the SLM was a mixed mode given by Equation (44). The mixed mode beam propagates to the lens $L1$, and then finally to the plane of the camera where the output profile is captured.

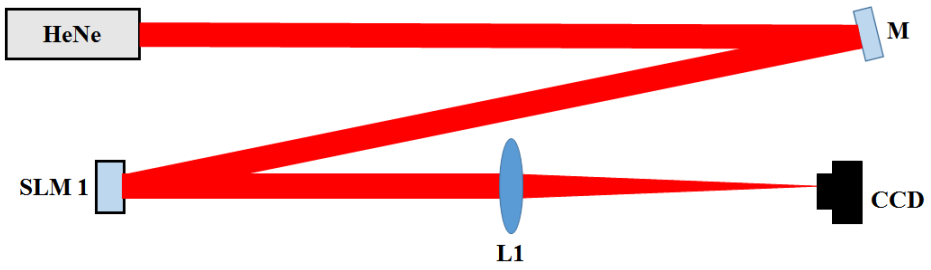

Figure 29: A schematic of the experimental set-up used to create the coherent superposition of Gaussian and vortex modes.

4.4 Results and Discussion

The superposition (mixed) mode was captured at the plane of the camera and possess a profile that gradually changes with the displacement of the singularity. The hologram singularity was displaced from the origin and studied for movements along the x-axis, y-axis, xy-axis and along a circle. The intensity distributions produced are depicted by Figure 30.

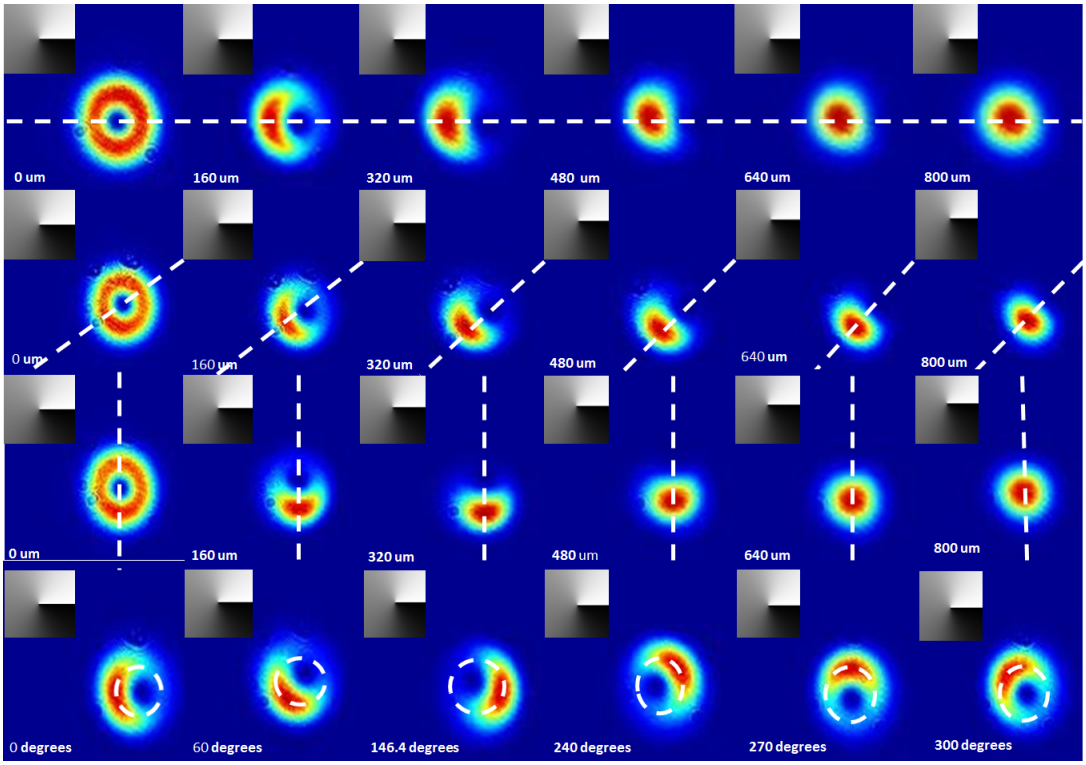

Figure 30: Intensity and phase distributions of off-axis vortex beams with off-axis displacement of the singularity given in white writing. When the central phase singularity of the hologram is not displaced, we get a normal symmetric vortex beam. When the central phase singularity of the hologram is displaced off the optical axis of the incident laser beam, an asymmetric vortex beam is produced.

For the x-axis, y-axis, and xy-axis displacements, it is evident that the beam starts off as a pure vortex mode with a symmetric structure. As the singularity displacement increases, the mode produced gradually changes into an off axis vortex and finally when the displacement is too big, it becomes a Gaussian mode. Basically, the weighting of the vortex mode decreases with singularity displacement and that of the Gaussian increases with the singularity displacement. For angular displacements of the hologram singularity, an off-axis vortex beam was produced but the degree of asymmetry of the vortex is relatively constant.

Our investigation revealed that the vortex structure appeared and disappeared as the displacement of the hologram singularity is varied, and that the degree of asymmetry of the superposition mode depends on the magnitude of the singularity displacement from the origin. It would be

appropriate to know the correspondence between the beams characteristics and the constituent modes to help understand the misalignment effects in different applications, and also to enhance the possibilities of applicability. Further analysis of off-axis vortex beams was conducted, and is presented in the following chapter.

4.5 Summary

We have experimentally generated a beam which is a superposition of Gaussian and vortex modes, and observed the beams transformation with different displacements of the holograms singularity point. When the singularity is displaced off the propagation axis of the incoming beam, the output vortex transforms from the vortex mode into a Gaussian mode for linear displacements of the singularity point. When off-axis displacement of the singularity is larger, you can ignore its impact of central phase singularity. Further studies on off-axis vortex beams are presented in the succeeding chapter.

References

[1] H. He, M.E.J. Friese, N.R. Heckenberg, H. Rubinsztein-Dunlop, Direct observation of transfer of angular momentum to absorptive particles from a laser beam with a phase singularity, Phys. Rev. Lett. 75 (1995) 826–829.

[2] N. B. Simpson, K. Dholakia, L. Allen, M. J. Padgett, Mechanical equivalence of spin and orbital angular momentum of light: an optical spanner, Opt. Lett. 22 (1997) 52–54.

[3] T. A. Nieminen, J. Higuet, G. Knoner, V. L. Y. Loke, S. Parkin, W. Singer, N.R. Heckenberg, H. Rubinsztein-Dunlop, Optically driven micromachines: progress and prospects, Proc. SPIE 6038 (2006) 237–245.

[4] A. V. Carpentier, H. Michinel, and J. R. Salgueiro, Making optical vortices with computer-generated holograms, Am. J. Phys. 76 (10), October 2008.

[5] G. Anzolin, F. Tamburini, A. Bianchini, and C. Barbieri, Method to measure off-axis displacements based on the analysis of the intensity distribution of a vortex beam, Physical Review A 79, 3 (2009)

[6] L. Allen, M. W. Beijersbergen, R. J. C. Spreeuw, and J. P. Woerdman, "Orbital angular momentum of light and the transformation of Laguerre-Gaussian modes," Phys. Rev. A 45, 8185–8190 (1992).

[7] J. B. Gotte, K. O'Holleran, D. Preece, F. Flossmann, S. Franke-Arnold, S. M. Barnett and M. J. Padgett, Light beams with fractional orbital angular momentum and their vortex structure, OPTICS EXPRESS 993,Vol. 16, No. 2, 2008.

[8] I. D. Maleev and G. A. Swartzlander, Jr., Composite Optical Vortices, J. Opt. Soc. Am. B, Vol. 20, No. 6, 2003.

5 Measurements with Off-Axis Vortex Beams

An off-axis vortex is a superposition of vortex and Gaussian modes, and its mode content is affected by the position of the singularity point. We have conducted a study of the mode structure of an off-axis vortex beam and put forward two methods to quantify its consituent modes. One method is based on the measurement of the intensity ratio, and the other is based on modal decomposition. Both techniques show that the mode of an off-axis vortex transforms from a pure vortex mode into a pure Gaussian mode as the singularity point is moved away from the beam's centre for movements along the $x-$axis, $y-$axis and $xy-$axis; and the mode is invariant for angular displacements of the singularity point.

5.1 Introduction

Optical vortex beams describe a wave field with wavefront dislocations [1]; and amplitude that vanishes at its axis while the phase becomes indefinite [2]. A vortex beam can be produced when a Gaussian beam is reflected from an SLM encoded with a spiral phase hologram. An off-axis vortex is formed when the dislocation of the phase mask is shifted relative to the axis of the input Gaussian.

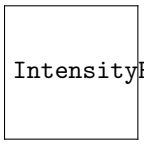

Figure 31: An off-axis vortex beam produced when there is a mismatch between the axis of an input Gaussian beam and a spiral hologram's singularity point. The white 'crosses' in (a) show the position of the two peak values I_1 and I_2 in (b).

In this study, we investigate the change in the mode structure with shifting singularity point. Two different techniques utilizing a SLM were applied to perform measurements and quantify the mode structure of an off-axis vortex. The first method is called the intensity ratio method, and involves finding the intensity ratio of the two peak values, as illustrated by Figure 31, then the mode content of the field can be deduced from the analysis of the intensity ratio. This ratio varies from one to zero as the vortex is transformed from a symmetric pure vortex mode to a pure Gaussian mode, respectively.

The second method applied in this study is called modal decomposition. Techniques to decompose light have been known for a very long time [3], and have been applied to the problem of studying the structure and propagation characteristics of laser beams [16, 17]. The modal decomposition expresses the field distribution as a linear combination of fundamental modes each weighted with a complex coefficient. These coefficients give intuitive information about an optical field. In practice, modal decomposition is accomplished by performing an inner product of the incoming field with a suitable computer generated match-filter, and for this case that is a mathc filter with azimuthal phase variation that is a complex conjugate of the mode being analyzed. The inner product yields an intensity signal at the Fourier plane from which the constituent modes of the beam are inferred.

This research provide an intuitive understanding of the interaction between a spiral phase mask and the background field; also on the relationship between the structure and dislocation position of the output vortex. The sensitivity of a vortex beam to displacements of the input beam has been proposed as an indicator of nanometric shifts in a speckle pattern [4] or to be used as a non-interferometric method for the correction of small surface deviations on spatial light modulators

[5].

5.2 Theory

In this section we define the field of an off-axis vortex in relation to each method that will be used to extract the constituent modes.

5.2.1 Intensity Ratio

The off-axis displacement of the input Gaussian beam with respect to the singularity of a spiral hologram produces an asymmetric far field intensity. Using the $z-$axis as the distance along the optical axis, the field of a superposition of vortex and Gaussian modes has been defined previously under section 4.2 and is defined by the equation;

$$U(r,x,y,z) = \alpha\Big[exp\Big(\frac{-r^2}{\omega(z)^2}\Big)\Big] + \beta\Big[(x+iy)\times exp\Big(\frac{-r^2}{\omega(z)^2}\Big)\Big], \tag{45}$$

The intensity of the superposition field is found to be,

$$\begin{aligned} I &= |U\times U^*|^2 \\ &= \alpha exp\Big(-\frac{r^2}{w(z)^2}\Big) + exp\Big(-i\theta r - \frac{r^2}{w(z)^2}\beta\Big)^2, \end{aligned} \tag{46}$$

where U^* is the complex conjugate of the superposition field. The spatial intensity distribution and the mode content of this mixed mode beam is unique for a given combination of the weighting coefficients α and β. Finding the first derivative dI/dr of this equation and solving for r, we find the positions of the two peaks, which are:

$$r_1 = \frac{-e^{i\theta}\alpha - \sqrt{e^{2i\theta}\alpha^2 + 2w(z)^2\beta^2}}{2\beta} \tag{47}$$

and

$$r_2 = \frac{-e^{i\theta}\alpha + \sqrt{e^{2i\theta}\alpha^2 + 2w(z)^2\beta^2}}{2\beta}. \tag{48}$$

Subtituting these position values into total the intensity equation (46) we find the intensities I_1 and I_2 at positions r_1 and r_2 respectively:

$$\begin{aligned} I_1 &= exp\Big(-\frac{2r_1^2}{w(z)^2} - 2i\theta\Big)\times(\alpha e^{i\theta} + \beta r_1)^2 \\ &= exp\Bigg[-\frac{\Big(-e^{i\theta}\alpha - \sqrt{e^{2i\theta}\alpha^2 + 2w(z)^2\beta^2}\Big)^2 - 2i\theta}{2w(z)^2\beta^2}\Bigg]\times \\ &\Bigg[e^{i\theta}\alpha + \frac{1}{2}\Big(-e^{i\theta}\alpha - \sqrt{e^{2i\theta}\alpha^2 + 2w(z)^2\beta^2}\Big)\Bigg]^2 \end{aligned} \tag{49}$$

and

$$
\begin{aligned}
I_2 &= exp(-\frac{2r_2^2}{w(z)^2} - 2i\theta)(exp(i\theta)\alpha + r_2\beta)^2 \\
&= exp\Bigg[- \frac{\Big(- e^{i\theta}\alpha + \sqrt{e^{2i\theta}\alpha^2 + 2w(z)^2\beta^2}\Big)^2 - 2i\theta}{2w(z)^2\beta^2}\Bigg] \times \\
&\Bigg[e^{i\theta}\alpha + \frac{1}{2}\Big(- e^{i\theta}\alpha + \sqrt{e^{2i\theta}\alpha^2 + 2w(z)^2\beta^2}\Big)\Bigg]^2 .
\end{aligned}
\tag{50}
$$

The ratio of these intensities is given by

$$
\begin{aligned}
\frac{I_2}{I_1} &= \left(\frac{\sqrt{e^{2i\theta}\alpha^2 + 2\omega^2\beta^2} + e^{i\theta}\alpha}{\sqrt{e^{2i\theta}\alpha^2 + 2\omega^2\beta^2} - e^{i\theta}\alpha}\right)^2 \times exp\frac{e^{2i\theta}\alpha\sqrt{e^{2i\theta}\alpha^2 + 2\omega^2\beta^2}}{\omega^2\beta^2} \\
&= \left(\frac{\sqrt{R^2+2}+R}{\sqrt{R^2+2}-R}\right)^2 \times exp\Big(2R\sqrt{R^2+2}\Big)
\end{aligned}
\tag{51}
$$

where $R = \frac{\alpha e^{i\theta}}{\beta w(z)}$. The complete derivation of this ratio can be found in the appendix.

5.2.2 Modal Decomposition

An electromagnetic wave can possess single or multiple modes. Modal decomposition is an intuitive approach for beam characterization; it provides fundamental insights into the nature of an electromagnetic wave and its propagation [6]. An arbitrary optical field $U(r)$ in equation (45) can be described as a superposition of a finite number of basis functions $\psi_n(r)$, called the modes, each weighted with a complex expansion coefficient c_n, as,

$$
U(r) = \sum_{n=1}^{n_{max}} c_n\psi_n(r). \tag{52}
$$

The eigenmodes of the field U form an orthogonal set, and thus satisfy the orthonormal property;

$$
\langle\psi_n|\psi_m\rangle = \int\int_{R^2} d^2r\psi_n^*(r)\psi_m(r) = \delta_{nm}, \tag{53}
$$

and the mode coefficients c_n are uniquely determined by the inner product of the optical field U and the corresponding eigenmode, i.e.

$$
c_n = \langle\psi_n|U\rangle = \int\int_{R^2} d^2r\psi_n^*(r)U(r) = \rho_n exp(i\Delta\phi_n). \tag{54}
$$

where (ρ_n) is the modal weight and $\Delta\phi_n$ is the modal phase. The mode content of the field U can be deduced from the complex expansion coefficients c_n of this inner product relation; and can experimentally measured in an optical set-up. The superposition field U can be created when a Gaussian beam is reflected from the SLM that is encoded with a spiral phase hologram that possesses displaced singularity point; and the mode distribution $\psi_n^*(r)$ can be programmed in the form of a correlation (or match) filter on to another SLM. The match filter was encoded with a

transmission function given by;

$$T(r) = \psi_n^*(r), \tag{55}$$

where $\psi_n^*(r)$ is the complex conjugate of the field to be detected. For the squared absolute values of c_n the following relation holds,

$$\sum_{n=1}^{n_{max}} |c_n|^2 = \sum_{n=1}^{n_{max}} (\rho_n^2) = 1; \tag{56}$$

and the inner product yields a far field on axis intensity that is proportional to (ρ_n^2).

5.3 Experimental Set-up and Methodology

The experimental set-up to measure a field which is a superposition of Gaussian and vortex modes is depicted in Figure .32. A HeNe laser (633 nm wavelength) was expanded through a telescope with a 5× magnification and directed onto a SLM (SLM 1: HoloEye, PLUTO-VIS, with 1920×1080 pixels of pitch $8\mu m$ and calibrated for a 2π phase shift). The superposition modes were produced when a Gaussian beam was incident on with various spiral holograms having a displaced singularity point on the LCD of the first SLM (SLM 1). At the Fourier plane of this SLM, the transverse profiles of the corresponding superimposed modes were captured for the analysis of intensity ratio method.

Figure 32: The experimental setup used for modal decomposition of an off-axis vortex.

For modal decomposition, the resulting superposition field from SLM 1 was then directed to the second SLM (SLM 2: same characteristics as SLM 1) which was encoded with a match filter for executing the modal decomposition by performing an inner product of the incoming field with the match filter. A match filter of a vortex mode ($l = 1$) was encoded on to SLM 2, while various weightings of the superposition field were produced with holograms possessing displaced singularity points on SLM 1. The same procedure was repeated with SLM 2 encoded a Gaussian modes match filter. The output correlation signal from SLM 2 was directed to the Fourier transforming lens with focal length of 500 mm, and finally captured with a CCD camera at the focal plane of this lens.

The mode content of the superposition field was determined from the measurement of the intensity distribution at a single on-axis location on the output correlation signal; realised by using an aperture. The aperture selection option provided by beam gauge software was used, thus enabling the measurement of the intensity distribution within the aperture. When the superposition field was the inverse of the match filter, beam gauge measured a non-zero on-axis intensity in the correlation signal and correspondingly a non-zero modal weighting. When the superposition field was not the inverse of the match filter, the output correlation signal at the Fourier plane had zero on-axis intensity and correspondingly a zero modal weighting.

5.4 Results and Discussion

In our experiments the phase singularity of the holograms was displaced from 0 to 10 pixels along x-axis, y-axis and xy-plane. For angular displacement, the singlularity was displaced from 0 to 360 degrees along a circle of radius of 10 pixels.

5.4.1 Intensity Ratio

Asymmetric superposition fields were produced experimentally, and the numerical values of the intensity of the peaks were found and the intensity ratio R was calculated for different displacements of the singularity point.

The relationship between the intensity ratio and singularity displacements are plotted, and it can be seen in Figure 33 that the intensity ratio increases exponentially from 0 to 1 for movements along x-axis, y-axis and xy-plane. These results are in perfect agreement with the theory (solid line). For large singularity displacements, the smaller peak becomes invisible and the beam profile only possesses one peak value; thus implies that the beam is now a Gaussian profile. The ratio R is proportion to $\frac{\alpha}{\beta}$, as the ratio increases from minimum value to maximum value; the weighting of Gaussian α increases while that of the vortex decreases.

Figure 33: The Ratio of the peak intensities plotted against the singularity displacement along (a) the x-axis, (b) the y-axis, (c) the xy-axis and (d) circle.

Angular displacement of the beams singularity was achieved by moving the hologram singularity along a circle of radius 10 pixels thus increasing the angular displacement θ. The intensity ratio for this case is given by Figure 33, and the theoretical intensity ratio remains constant while there are small fluctuation in the experimental results. The reason for this difference is that the experimental results cannot be as perfect as theory; the intensity ratio for the centred symmetric vortex beam was not one, therefore this tells us that under perfect conditions the topological charge value does not change with angular displacement of the beam's singularity at constant radial position.

5.4.2 Modal Decomposition

Measurements on the output correlation signal, captured by the CCD camera, were made in order to determine the mode content of an off-axis vortex. Using beam gauge, an aperture was placed around the central region of the correlation signal inorder to measure on-axis intensity. When the superposition field was the inverse of the match filter, beam gauge measured a non-zero on-axis intensity on the correlation signal and correspondingly a non-zero modal weighting. When the superposition field was not the inverse of the match filter, the output correlation signal at the Fourier plane had zero on-axis intensity and correspondingly a zero modal weighting.

The weightings of the two modes present in the superposition field were plotted as a function of singularity displacement from the origin, shown in the bar graphs in Figure 34. The phase singularity on the holograms was displaced from 0 to 10 pixels along x-axis, y-axis and xy-plane. The results of modal decomposition show that when the singularity is exactly on-axis, the resulting beam is a pure vortex mode, this is evident from the maximum weighting of the vortex (l=1

mode), and minimum weighting for the Gaussian (l=0 mode). As the singularity is displaced off-axis, the Gaussian weighting increases and the vortex weighting decreases, and at our chosen maximum displacement from the origin (10 pixels), the Gaussian weighting becomes maximum and that of the vortex beam becomes minimum.

For angular displacements, the singlularity was displaced from 0 to 360 deg along a circle of radius of 10 pixels. The variation of mode weightings was small; and the Gaussian mode dominated throughout all angular movements. This shows that the mode content of the superposition field is not affected by angular movements. A small decrease in the Gaussian weighting and a small increase in the vortex weighting was present for some displacements. The reason for this is that experimental results were not perfect; and the weightings never reached a point where they were exactly zero or eaxactly one. Ideally, when a vortex is centered on the singularity, we should get a weighting of zero for the Gaussian and a weighting of one for the vortex.

Figure 34: The weighting of the two azimuthal modes plotted against the displacement of the singularity along (a) the x-axis, (b) the y-axis, (c) the xy-axis and (d) circle.

5.5 Summary

We have presented and discussed two methods to measure off-axis optical vortex beams, intensity ratio and modal decomposition. The measurements revealed that the superposition field changes from a vortex mode into a Gaussain mode with singularity displacement from the origin. These results enable the control of the weightings of each of the superimposed modes.

References

[1] M. V. Vasnetsov, V. V. Slyusar, M. S. Soskin, Mode Separator for a Beam with Off-axis Optical Vortex, Quantum Electronics, 31(5) 464-466(2001).

[2] M. Vasnetsov and K. Staliunas, Eds., Optical Vortices, Nova Science, Huntington, NY, USA, 1999

[3] J. W. Goodman, Introduction to Fourier Optics, McGraw-Hill Publishing Company, 1968.

[4] W. Wang, T. Yokozeki, R. Ishijima, M. Takeda, and S. G. Hanson, Optical Vortex Metrology Based on the Core Structures of Phase Singularities in Laguerre-Gauss transform of a Speckle Pattern, Opt. Expr. 14, 10195 (2006).

[5] A. Jesacher, A. Schwaighofer, S. Furhapter, C. Maurer, S. Bernet, and M. Ritsch-Marte, Wavefront correction of spatial light modulators using an optical vortex image, Opt. Expr. 15, 5801 (2007).

[6] T. Kaiser, D. Flamm, S. Schroter and M Duparre, Complete Modal Decomposition for Optical Fibers using CGH Based Correlation Filters, Opt. Expr., Vol. 17, No. 11 (2009).

[7] G. Indebetouw, "Optical Vortices and Their Propagation," J. Mod. Opt. 40, 73–87 (1993).

[8] F. S. Roux, Coupling of Noncanonical Optical Vortices, J. Opt. Soc. Am. B 21 (2004) 664-670.

[9] D. Rozas, C. T. Law, and G. A. Swartzlander, "Propagation Dynamics of Optical Vortices," J. Opt. Soc. Am. B 14, 3054-3065 (1997)

[10] Y. S. Kivshar and E. A. Ostrovskaya, "Optical Vortices: Folding and Twisting Waves of Light," Opt. Photonics. News 12(4), 24–28 (2001)

[11] L. Torner, D.V. Petrov, Splitting of Light Leams with Spiral Phase Dislocations into Solitons in Bulk Quadratic Nonlinear Media, J. Opt. Soc. Am. B 14 (1997), 2017-2023.

[12] D. V. Petrov, Second harmonic generation by optical beams with edge phase dislocations, Optics Communications 192(1–2), 2001, pp. 101–106.

[13] A.P. Sukhorukov, A. Kalinovich, G. Molina-Terriza, L.Torner, Superposition of noncoaxial vortices in parametric wave mixing, Phys Rev. E 66, (2002)036608].

[14] E. Tervonen, J. Turunen and A. Friberg, "Transverse laser mode structure determination from spatial coherence measurements: experimental results," Appl. Phys. B 49, 409-414 (1989).

[15] A. Cutolo, T. Isernia, I. Izzo, R. Pierri, and L. Zerni, "Transverse mode analysis of a laser beam by near- and far-field intensity measurements," Appl. Opt. B 34, 7974-7978 (1995).

[16] M. Santarsiero, F. Gori, R. Borghi, and G. Guattari, "Evaluation of the modal structure of light beams composed of incoherent mixtures of Hermite-Gaussian modes," Appl. Opt. B 38, 5272-5281 (1999).

[17] X. Xue, H. Wei, and A. G. Kirk, "Intensity-based modal decomposition of optical beams in terms of HermiteGaussian functions," J. Opt. Soc. Am. A 17, 1086-1091 (2000).

6 The Propagation of Vortex and LG Beams

We have studied and made comparisons on the properties of optical vortex beams and Laguerre Gaussian beams propagating through free space under the same conditions. Specifically, we investigated the beam size dependence on propagation distance. This was realized digitally, by employing an SLM encoded with holograms to produce a beam that is propagated onto various planes. The results show an excellent agreement between theory and experiment for beam radius variation with propagation distance. The beams intensity decreases with propagation distance for both beams, and the overall beam spreading of a vortex beam is less than that of an LG beam for the distances investigated.

6.1 Introduction

One characteristic of laser beams is that they are highly directional [1] and thus propagate as a narrow beam. However, laser beam studies have been found that the initial beam properties (beam shape, phase, coherence, size etc.) are strongly affected by propagation [2]-[6]. The study of their propagation dynamics enables exploring fundamental properties of optical vortices and has led to the discovery of knots [7] in the trajectory of the singularities as the light propagates.

Propagation of laser beams has important applications in many areas including Free Space Optical Communications (FSOC) [8, 9], Laser Detection and Ranging (LADAR) systems, Light Detection and Ranging (LIDAR), and remote sensing and imaging [11]. In laser applications, such as military and communication, it is necessary to monitor the laser profile continuously during the laser operation. The optimization of these systems relies on the understanding of the propagation dynamics of laser beams.

Many techniques have been applied to the problem of studying the structure and propagation characteristics of laser beams [14] - [17]. The experimental study of free space propagation properties of laser beams normally involves a mechanical scanning procedure, used by Filippo Cardano, et. al [12], which requires continuously moving the camera, adjusting components for proper alignment; and then capturing the beam profile at each plane along the propagation direction in the far field, thereafter the required information is obtained from the experimental data. The challenge with this procedure is that it requires a high degree of alignment, is time consuming and prone to errors; especially for large distances, unwanted environmental fluctuations would need to be accounted for.

A fast and easily applicable technique is desired; and is provided for by the SLM technology. The beam propagation required can be attained with the SLM-based digital propagation method which displays a hologram with the free space propagation factor; and therefore, a camera at a fixed point behind the SLM captures images of a beam that is artificially propagated to a distance corresponding to the propagation factor of the uploaded hologram. With this method, even experiments for large propagation distances can be made with ease.

We present an experimental and theoretical study of the propagation dynamics of vortex and LG beams with topological charge of $l = +1$ propagating along the same distance in free space. These beams are generated and propagated by an SLM and then analysed using various methods. It was found that the beam radius increases with propagation distance, and that the overall spreading of the Vortex beam is less than that of an LG beam.

6.2 Theory

The most common means of producing optical vortices are computer-generated holograms (CGHs); since they provide a flexible way to encode an arbitrary wave function by modulating only the phase

of the hologram [13]. Optical vortex beams are characterised by the azimuthally-varying phase factor $exp(il\theta)$, which gives rise to the OAM carried in the optical vortex. The field distribution of an optical vortex can be expressed in the form;

$$U(r,\theta) = u_0(r)exp(il\theta). \tag{57}$$

For an optical vortex, which is an approximation of an LG mode, the initial field is given by [14],

$$u_0(r) = exp(\frac{-r^2}{\omega(z)^2}). \tag{58}$$

To generate the field of an optical vortex using a Gaussian beam as our initial reference beam, we need only generate a hologram which represents the following transmission function

$$t(\theta) = exp(il\theta). \tag{59}$$

A Laguerre-Gaussian mode has a field given by:

$$\begin{aligned} U_{p,l}(r,\phi,z) = \frac{1}{\omega(z)}\sqrt{\frac{2p!}{\pi(\,|l|+p)!}}exp\Big[i(2p+|l|+1)\psi(z)\Big] \;\times \left(\frac{\sqrt{2}r}{\omega(z)}\right)^{|l|} \times \\ L_p^l\Big(\frac{2r^2}{\omega^2(z)}\Big)exp\Big[-ik\frac{r^2}{2q(z)} + il\theta\Big]. \end{aligned} \tag{60}$$

For the Laguerre-Gaussian mode, he transmission function is;

$$t(r,\theta) = exp(i\cos(l\theta - \frac{2\pi}{\Lambda}r\cos\theta)), \tag{61}$$

where Λ is the grating spacing. In this research, designs of CGHs for producing LG modes were created by mathematically interfering a plane wave with an optical vortex and the output beam reflected from the SLM was diffracted into multiple orders of optical vortices of distinct topological charge.

A laser beam's divergence can be measured using a technique that involves measuring the beam diameter at different planes along the propagation axis. This process is tedious, and prone to errors. Free space propagation can be made with ease using a method which applies a propagation operator factor z to the wave function, and therefore calculates the wave function at a distance z further along the beams propagation path. In this study, the holograms encoded on the SLM were used for both the generation and propagation of these beams, and a camera at a fixed point behind the SLM captured images of an artificially propagated beam.

The intensity of a vortex beam is defined by [15],

$$I = r^{2l} \times exp\Big(\frac{-2r^2}{\omega(z)^2}\Big). \tag{62}$$

while the intensity of a Laguerre-Gaussian beam is defined by,

$$I = \frac{2}{\pi\omega(z)^2 l!}\left(\frac{r\sqrt{2}}{\omega(z)}\right)^{2l} exp\left(\frac{2r^2}{\omega(z)^2}\right), \tag{63}$$

where $\omega(z) = \sqrt{\omega_0^2\left(1+\frac{z^2}{Z_R}\right)}$ is the beam radius at propagation distance z, and Z_R is the Rayleigh range. The intensity profiles of LG and vortex beams are similar, but the spatial dynamics that occur with propagation shows remarkable differences. The radius of maximum optical intensity,

r_l , given by:

$$r_l = \omega(z)\sqrt{\frac{l}{2}}. \tag{64}$$

From which we can deduce that the beam diameter is given by

$$D_l = 2\omega(z)\sqrt{\frac{l}{2}}. \tag{65}$$

The diameter, $D_l = 0$ for $l = 0$. In this study, the optical vortex charge was $l = 1$, therefore at the plane of the beam waist, the diameter is,

$$D_l = 2\omega_0\sqrt{\frac{1}{2}} = \sqrt{2}\omega_0. \tag{66}$$

Measuring the beam diameter at different planes along the propagation axis gives a measure of the beams divergence.

6.3 Experimental Set-up and Methodology

The experimental set-up for digital propagation is depicted by Figure 36, and consists of a HeNe laser emitting a wavelength of 633 nm. The beam is then expanded by a telescope made of lenses of focal lengths $f_1 = 50$ mm and $f_2 = 500$ mm. The input Gaussian beam was modified by holograms with various propagation factors on the SLM, then the output intensity profile was pass through one-to-one imaging lenses (f_3 and f_4), both with focal length of $f = 250$ mm. The mirror (M) was used to redirected the beam to the Fourier transforming lens of focal length $f_5 = 500$ mm, and finally the beam was incident on the camera for viewing and capturing the output profile.

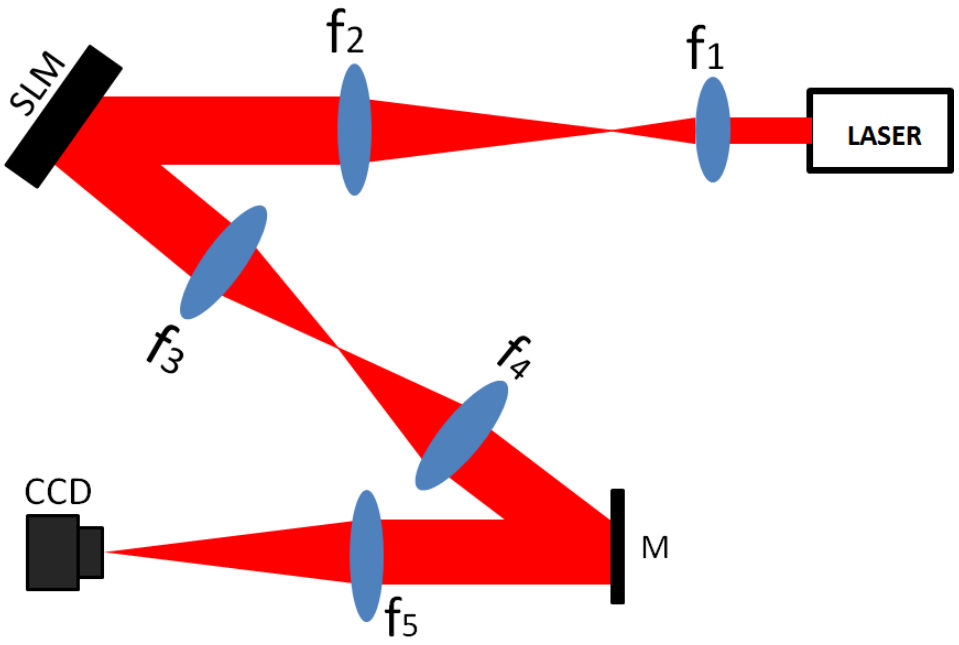

Figure 35: The experimental set-up used for digital propagation of LG and Vortex beams.

It should be noted that holographic masks encoded on the Holoeye pluto phase-only SLM were used for both the generation and propagation of these beams. The incident Gaussian was modified by holograms programed and encoded on the SLM with different propagation factors; therefore beams corresponding to different far field distances were observed at the focus of the Fourier transforming lens.

The output intensity profiles were captured for different propagation distances from $z = 0$ mm to $z = 1000$ mm using a CCD camera. These images were further analysed to determine and compare the intensity's spatial evolution and vortex diameter dependence on propagation distance.

6.4 Results and Discussion

Digitally propagated LG beams and vortex beams, were produced for propagation distances from $z = 0$ mm to $z = 1000$ mm. The images of holograms and transverse intensity patterns captured by a CCD camera, are shown for different propagation factors in Figure 37 and Figure 38. Beam intensity images were captured every 200 mm of the total 1 m propagation distance. The theoretical profiles of vortex and LG beams were generated in Matlab using Equations 62 and 63, respectively. The colours on these profiles range from red to dark blue representing intensity variation from maximum to minimum. The beam diameter along the propagation axis increases with propagation distance for both LG and Vortex beam. The is due to diffractive spreading of a beam in free space propagation. These results show an excellent agreement between theory and the experiment for beam radius variation with propagation distance.

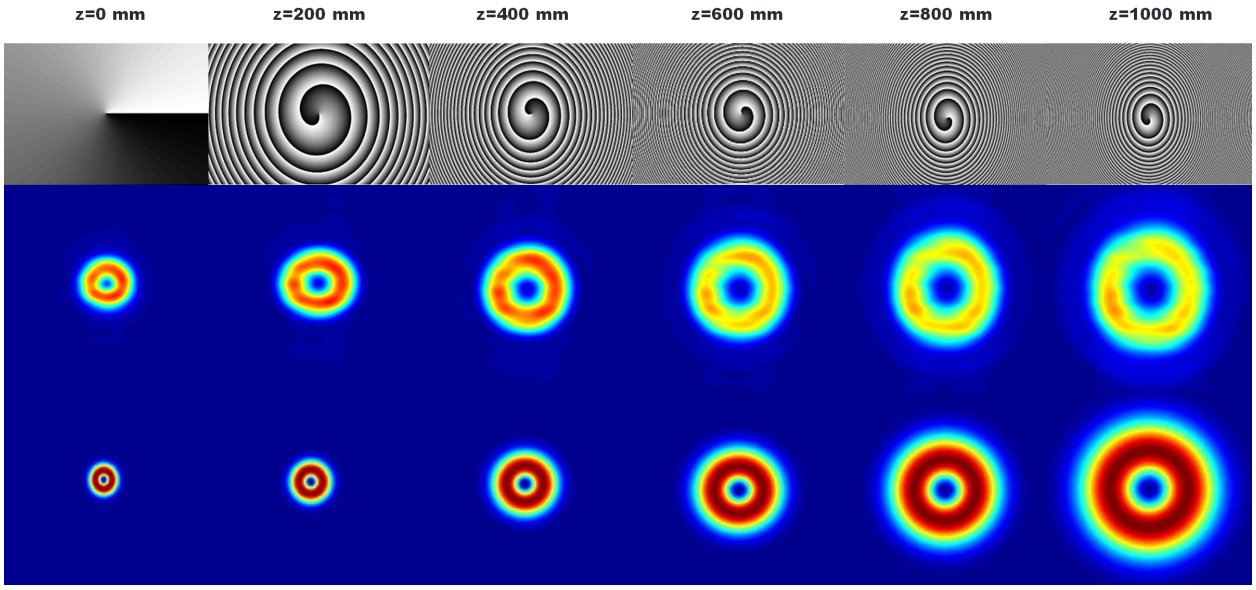

Figure 36: The intensity patterns captured by a CCD camera are shown for different propagation factors (z values). The first row shows typical holograms for producing vortex beams, encoded with different propagation factors. The vortex beams produced experimentally at the focus of the Fourier transforming lens and theoretically produced vortex beams are depicted on the second and third row, respectively.

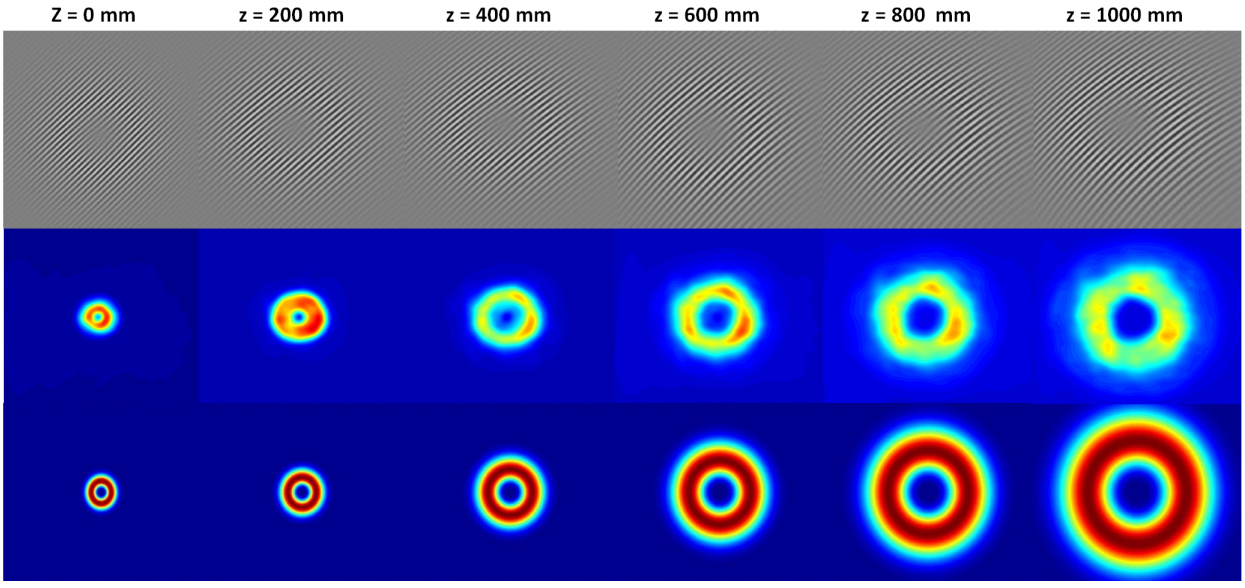

Figure 37: The typical holograms (first row) for producing LG beams propagated to various z planes together with experimentally generated LG beams (second row) at the focus of the Fourier transforming lens and theoretically generated profiles (third row).

The captured images of propagation of vortex and LG beams of topological charge $l = 1$ were converted into an ascii file format, so as to plot the cross-section. A cross-section of the intesity profile along the centre of the beam was plotted as a function of radial distance (represented by pixel number). The result reported in Figure 39 show the intensity patterns measured at the camera plane. At $z = 0$ mm, the vortex and LG intensities are almost superimposed. A difference is evident at $z = 500$ mm and $z = 1000$ mm, the diameter of an LG beam is bigger than that of a vortex. This show that the averall spreading of a vortex is less than that of an LG beam in free space; therefore a vortex is more stable in free space propagation as it suffers less spreading.

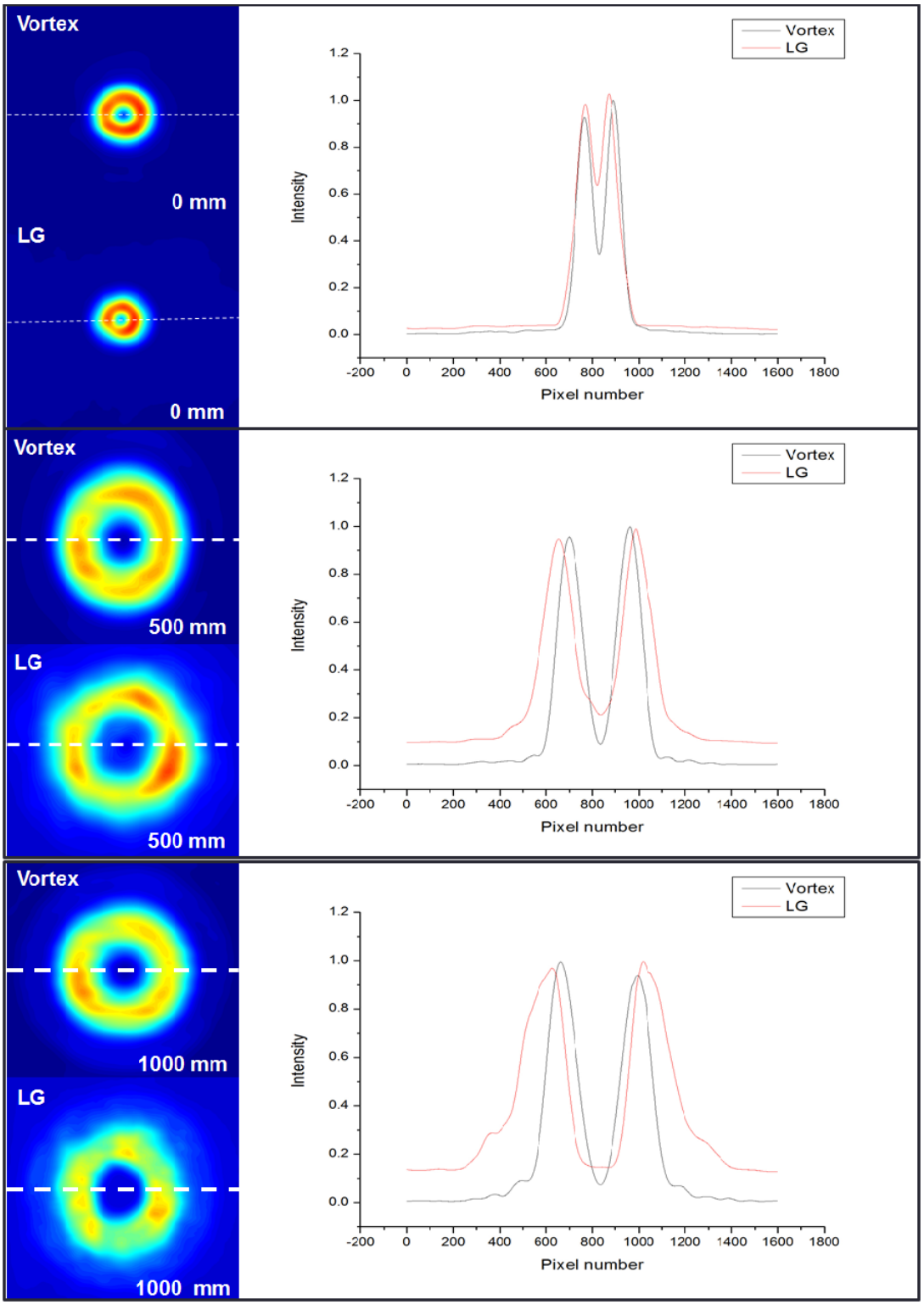

Figure 38: Comparisons between cross sections of the experimental far-field intensity of a vortex beam (black line) and LG beam (red line), for propagation distances $z = 0$ mm, $z = 500$ mm and $z = 1000$ mm.

The shape of the optical vortex does not have well defined edges; therefore its diameter can be defined in many different ways. In this study, the peak-to-peak distance was used to give a measure of beam diameter $D_l = 2\omega(z)\sqrt{\frac{l}{2}}$. The peak-to-peak distance was measured and then plotted as a function of propagation distance in origin. The results, depicted by Figure 39, show that the beam diameter, for both vortex and LG beams, is a minimum for propagation distance $z = 0$ mm, and that the LG beam diameter spreads more than the vortex beam for propagation distances from 200 mm onwards, therefore the overall beam spreading of a vortex beam is less than that of an LG beam for the distances investigated.

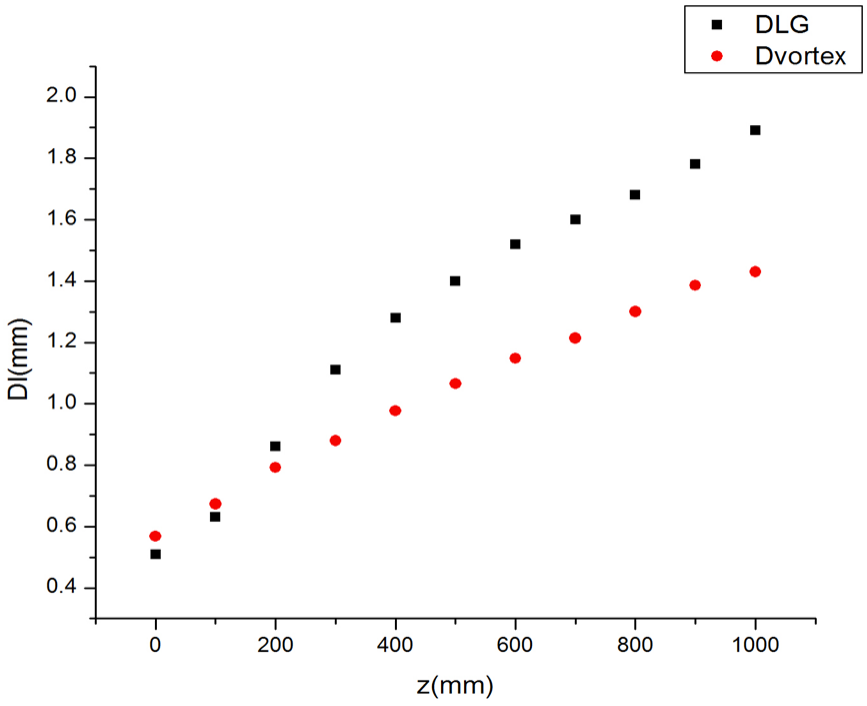

Figure 39: Experimental results of beam diameter D_l versus propagation distance z for vortex (red dots) and LG (black dots) beams.

6.5 Summary

We have presented a study of the vortex and LG beam profiles evolution as it propagates in free space. The free-space propagation of vortex beams and LG beams was experimentally investigated by making use of digital propagation. The beam diameter was measured at each plane of the propagation distances. Our results show that a vortex beam has less divergence compared to the LG beam; the differences between the vortex and LG beams grow with propagation displacement. These results indicates that the vortex is more stable than the LG in free space propagation, and such properties are useful for free space communication applications.

References

[1] M. Csele, Fundamentals of Light Sources and Lasers, John Wiley and Sons, Inc., Hoboken, New Jersey, 2004.

[2] H. Ruan, L. Wang, S. Wu, L. Liu and B. Zhou, Free Space Vortex Light by Diffraction of a Bessel Beam From Optical Fiber, IEEE Photonics Journal, Vol. 9, No. 4, 2017.

[3] M. P. J. Lavery, C. Peuntinger, K. Günthner, P. Banzer, D. Elser, R. W. Boyd, M. J. Padgett, C. Marquardt, G. Leuchs, Free-space propagation of high-dimensional structured optical fields in an urban environment, Sci. Adv. 3 (2017).

[4] Z. Chen, C. Li, P. Ding, J. Pu and D. Zhao, Experimental investigation on the scintillation index of vortex beams propagating in simulated atmospheric turbulence, Appl Phys B (2012) 107:469–472

[5] W. Zhu, J. Guan, F. Deng, D. Deng and J. Huang, The propagation properties of the first-order and the second-order Airy vortex beams through strongly nonlocal nonlinear medium, Optics Communications, 380 (2016) 434–441

[6] K. S. Morgan, J. K. Miller, B. M. Cochenour, W. Li, Y. Li, R. J. Watkins and E. G. Johnson, Free space propagation of concentric vortices through underwater turbid environments, J. Opt. 18 (2016) 104004.

[7] J. Leach, M. R. Dennis, J. Courtial, and M. J. Padgett, Vortex knots in light, New J. of Phys. 7, 1–11 (2005).

[8] A. Malik and P. Singh, "Free Space Optics: Current Applications and Future Challenges," International Journal of Optics, vol. 2015, Article ID 945483, 7 pages, 2015. doi:10.1155/2015/945483.

[9] D. Cornwell, Space-Based Laser Communications Break Threshold, Optics and Photonics News (2016), Accessed online, at: $https : //www.osa - opn.org/home/articles/volume_27/may_2016/features/space - based_laser_communications_breakthreshold/$

[10] H. Wille, M. Rodriguez, J. Kasparian, D. Mondelain, J. Yu, A. Mysyrowicz, R. Sauerbrey, J. P. Wolf and L. Wöste, Teramobile: A mobile femtosecond-terawatt laser and detection system, The European Physical Journal - Applied Physics, 20(3), 183-190 (2002).

[11] K. W. Rothe, U. Brinkmann, H. Walther, Applications of tunable dye lasers to air pollution detection: Measurements of atmospheric NO_2 concentrations by differential absorption, Appl. Phys. 3, 115-119 (1974).

[12] F. Cardano, E. Karimi, L. Marrucci, C. de Lisio, and E. Santamato, Generation and dynamics of optical beams with polarization singularities, Accessed online, at: $https : //arxiv.org/pdf/1211.4163.pdf$

[13] F. Venturi, R. Balboni, G. C. Gazzadi, M. Campanini, E. Karimi, and V. Grillo, S. Frabboni, R. W. Boyd, Generation with phase-and-amplitude electron holograms of Laguerre-Gauss beams with orbital angular momentum up to $200\hbar$, accessed from: $http : //dx.doi.org/10.1002/9783527808465.EMC2016.4914$.

[14] A. Y. Bekshaev, A. I. Karamoch, M. V. Vasnetsov, V. A. Pas'ko, M. S. Soskin, Structure of optical vortices produced by holographic gratings with "fork" geometry: Kummer beams Accessed online, at: $https : //arxiv.org/ftp/arxiv/papers/0906/0906.2619.pdf$

[15] S. G. Reddy, P Chithrabhanu, S. Prabhakar, A. Anwar, J. Banerji and R. P. Singh, Divergence of optical vortex beams, Accessed from: $http : //arxiv.org/pdf/1505.05993.pdf$

[16] L. Allen, M. W. Beijersbergen, R. J. C. Spreeuw and J. P. Woerdman, Orbital angular momentum of light and the transformation of Laguerre–Gaussian laser modes, Phys. Rev. A 45 8185–9, 1992.

[17] M. J. Padgett , F. M. Miatto , M. P. J. Lavery , A. Zeilinger and R. W. Boyd, Divergence of an orbital-angular-momentum-carrying beam upon propagation, New J. Phys. 17 (2015) 023011.

[18] D. Rozas, Generation and Propagation of Optical Vortices, PhD Thesis, Worcester Polytechnic Institute, 1999.

[19] A. Mani, M. Wang, and P. Moin, "Statistical description of the free-space propagation of highly aberrated optical beams," J. Opt. Soc. Am. A 23, 3027-3035 (2006).

[20] W. Cheng, J. W. Haus, and Q. Zhan, "Propagation of vector vortex beams through a turbulent atmosphere," Opt. Express 17, 17829-17836 (2009).

[21] A. V. Mamaev, M. Saffman, and A. A. Zozulya, Vortex Evolution and Bound Pair Formation in Anisotropic Nonlinear Optical Media, Physical Review Letters, Vol. 77, No. 22(1996).

[22] G. Ruffato, M. Carli, M. Massari and F. Romanato, Spiral phase plates for the generation of high-order LaguerreGaussian beams with non-zero radial index, Proc. of SPIE Vol. 9379, 937905 (2015).

[23] A. Y. Bekshaev, A. S. Bekshaev and K. A. Mohammed, Arrays of optical vortices formed by 'fork' holograms, Ukr. J. Phys. Opt., Volume 15, Issue 3 , 2014.

[24] A. A. Kovalev, V. V. Kotlyar, A. G. Nalimov, Nonparaxial optical vortices and Kummer laser beams, Optical Engineering, Vol. 52(9), 2013.

[25] L. A. Clark, Electron Vortex Beams: Production and Propagation, MSc. Thesis, University of York, 2012.

7 Conclusion and Future Work

In this thesis, we presented methods in which an SLM can be used to produce arbitrary beam profiles. In chapter 3, a beam shaping system based on a SLM and digital holograms was presented. After evaluation of different methods, it was obvious that the SLM based method is the most efficient. With the SLM based method, a Gaussian profile was modified to produce vortex, LG, and Bessel beams. The superposition of LG and Bessel beams was also produced. Experimental results were in good agreement with simulated counterparts. The superposition of Bessel beams were created, and their structure possess petals which rotate as the beam propagates in free space. The rotation of the petals was studied and it was found to be a linear rotation. In Chapter 4, off-axis vortex beams were generated and their intensity profile has an asymmetric intensity profile. Chapter 5 discusses two methods to measure off-axis vortex beams; modal decomposition and intensity ratio method. In Chapter 6, we presented a study of propagation properties of vortex and LG modes. These beams were propagated in free space and the dependence of vortex radius on propagation distance was also studied. It was found that the vortex radius increases with propagation distance for both types of beam and that an optical vortex beam is spreads less than the LG beam, we plan to apply the SLM beam shaping system to the optical tweezing system to trap and study micro-particles. In addition, we want to implement the SLM based beam shaping system for potential applications in biology and biomedical engineering.

A Appendix A: The derivation of an Off-Axis vortex Beam's Intensity Ratio

An off-axis vortex results when the axis of a Gaussian beam does not coincide with that of the phase hologram. An off axis Vortex has an asymmetric intensity profile that shows two different peaks along the direction of maximum asymmetry. These peaks vary in size with off-axis displacement of the holograms singularity point.

Intensity ratio derivation is given in the matheamtica note-book below.

This shows the derivation of the ratio I2 / I1

Ug : field of a gaussian
Uv : field of a vortex
UvInv : inverse field of a vortex

In[153]:=
```
Ug = Exp[ -r^2 / wz^2 ]
Uv = (r * Exp[i * θ]) * Ug
UvInv = Uv = (r * Exp[-i * θ]) * Ug
Utot = α * Ug + β * Uv
UtotInv = α * Ug + β * UvInv
Itot = Utot * UtotInv
```

Out[153]= $e^{-\frac{r^2}{wz^2}}$

Out[154]= $e^{-\frac{r^2}{wz^2}+i\theta}\, r$

Out[155]= $e^{-\frac{r^2}{wz^2}-i\theta}\, r$

Out[156]= $e^{-\frac{r^2}{wz^2}}\, \alpha + e^{-\frac{r^2}{wz^2}-i\theta}\, r\, \beta$

Out[157]= $e^{-\frac{r^2}{wz^2}}\, \alpha + e^{-\frac{r^2}{wz^2}-i\theta}\, r\, \beta$

Out[158]= $\left(e^{-\frac{r^2}{wz^2}}\, \alpha + e^{-\frac{r^2}{wz^2}-i\theta}\, r\, \beta\right)^2$

derivative of intensity wrt r

In[159]:=
```
dIdr = ∂r (e^(-2 r^2/wz^2 - 2 i θ) (e^(i θ) α + r β)^2)
```

Out[159]= $2\, e^{-\frac{2r^2}{wz^2}-2i\theta}\, \beta\, \left(e^{i\theta}\, \alpha + r\, \beta\right) - \frac{4\, e^{-\frac{2r^2}{wz^2}-2i\theta}\, r\, \left(e^{i\theta}\, \alpha + r\, \beta\right)^2}{wz^2}$

Solving to find r - values where dIdr = 0

In[160]:=
```
Solve[2 e^(-2 r^2/wz^2 - 2 i θ) β (e^(i θ) α + r β) - 4 e^(-2 r^2/wz^2 - 2 i θ) r (e^(i θ) α + r β)^2 / wz^2 == 0, r]
```

Out[160]= $\left\{\left\{r \to -\frac{e^{i\theta}\, \alpha}{\beta}\right\}, \left\{r \to \frac{-e^{i\theta}\, \alpha - \sqrt{e^{2i\theta}\, \alpha^2 + 2\, wz^2\, \beta^2}}{2\, \beta}\right\}, \left\{r \to \frac{-e^{i\theta}\, \alpha + \sqrt{e^{2i\theta}\, \alpha^2 + 2\, wz^2\, \beta^2}}{2\, \beta}\right\}\right\}$

In[161]:=
$$r0 = -\frac{e^{i\theta}\alpha}{\beta}$$

$$r1 = \frac{-e^{i\theta}\alpha - \sqrt{e^{2i\theta}\alpha^2 + 2\,wz^2\,\beta^2}}{2\beta}$$

$$r2 = \frac{-e^{i\theta}\alpha + \sqrt{e^{2i\theta}\alpha^2 + 2\,wz^2\,\beta^2}}{2\beta}$$

Out[161]=
$$-\frac{e^{i\theta}\alpha}{\beta}$$

Out[162]=
$$\frac{-e^{i\theta}\alpha - \sqrt{e^{2i\theta}\alpha^2 + 2\,wz^2\,\beta^2}}{2\beta}$$

Out[163]=
$$\frac{-e^{i\theta}\alpha + \sqrt{e^{2i\theta}\alpha^2 + 2\,wz^2\,\beta^2}}{2\beta}$$

Subtituting the r - values into total intensity to find the intensities I0, I1 and I2 at positions r0, r1 and r1 respectively

In[164]:=
$$I0 = e^{-\frac{2\,r0^2}{wz^2}-2i\theta}\left(e^{i\theta}\alpha + r0\,\beta\right)^2$$

$$I1 = e^{-\frac{2\,r1^2}{wz^2}-2i\theta}\left(e^{i\theta}\alpha + r1\,\beta\right)^2$$

$$I2 = e^{-\frac{2\,r2^2}{wz^2}-2i\theta}\left(e^{i\theta}\alpha + r2\,\beta\right)^2$$

Out[164]= 0

Out[165]=
$$e^{-\frac{\left(-e^{i\theta}\alpha-\sqrt{e^{2i\theta}\alpha^2+2\,wz^2\,\beta^2}\right)^2}{2\,wz^2\,\beta^2}-2i\theta}\left(e^{i\theta}\alpha + \frac{1}{2}\left(-e^{i\theta}\alpha - \sqrt{e^{2i\theta}\alpha^2 + 2\,wz^2\,\beta^2}\right)\right)^2$$

Out[166]=
$$e^{-\frac{\left(-e^{i\theta}\alpha+\sqrt{e^{2i\theta}\alpha^2+2\,wz^2\,\beta^2}\right)^2}{2\,wz^2\,\beta^2}-2i\theta}\left(e^{i\theta}\alpha + \frac{1}{2}\left(-e^{i\theta}\alpha + \sqrt{e^{2i\theta}\alpha^2 + 2\,wz^2\,\beta^2}\right)\right)^2$$

the ratio of the two maxima

In[167]:=
$$I2I1 = I2 / I1$$

Out[167]=
$$\left(e^{\frac{\left(-e^{i\theta}\alpha-\sqrt{e^{2i\theta}\alpha^2+2\,wz^2\,\beta^2}\right)^2}{2\,wz^2\,\beta^2}-\frac{\left(-e^{i\theta}\alpha+\sqrt{e^{2i\theta}\alpha^2+2\,wz^2\,\beta^2}\right)^2}{2\,wz^2\,\beta^2}}\left(e^{i\theta}\alpha + \frac{1}{2}\left(-e^{i\theta}\alpha + \sqrt{e^{2i\theta}\alpha^2 + 2\,wz^2\,\beta^2}\right)\right)^2\right) \Big/ \left(e^{i\theta}\alpha + \frac{1}{2}\left(-e^{i\theta}\alpha - \sqrt{e^{2i\theta}\alpha^2 + 2\,wz^2\,\beta^2}\right)\right)^2$$

In[168]:=
Simplify[%167]

Out[168]=
$$\frac{e^{\frac{2e^{i\theta}\alpha\sqrt{e^{2i\theta}\alpha^2+2\,wz^2\,\beta^2}}{wz^2\,\beta^2}}\left(e^{i\theta}\alpha + \sqrt{e^{2i\theta}\alpha^2 + 2\,wz^2\,\beta^2}\right)^2}{\left(-e^{i\theta}\alpha + \sqrt{e^{2i\theta}\alpha^2 + 2\,wz^2\,\beta^2}\right)^2}$$

The following manipulations were done to further simplify the equation that defines the ratio;

$$\frac{I_2}{I_1} = (\frac{\sqrt{e^{2i\theta}\alpha^2 + 2\omega^2\beta^2} + e^{i\theta}\alpha}{\sqrt{e^{2i\theta}\alpha^2 + 2\omega^2\beta^2} - e^{i\theta}\alpha})^2 \times exp\frac{e^{2i\theta}\alpha\sqrt{e^{2i\theta}\alpha^2 + 2\omega^2\beta^2}}{\omega^2\beta^2} \tag{67}$$

$$\frac{I_2}{I_1} = (\frac{\frac{1}{\omega\beta} \times \sqrt{e^{2i\theta}\alpha^2 + 2\omega^2\beta^2} + e^{i\theta}\alpha}{\frac{1}{\omega\beta} \times \sqrt{e^{2i\theta}\alpha^2 + 2\omega^2\beta^2} - e^{i\theta}\alpha})^2 \times exp\frac{\frac{1}{\omega^2\beta^2} \times e^{2i\theta}\alpha\sqrt{e^{2i\theta}\alpha^2 + 2\omega^2\beta^2}}{\frac{1}{\omega^2\beta^2} \times \omega^2\beta^2} \tag{68}$$

$$\frac{I_2}{I_1} = (\frac{\sqrt{\frac{e^{2i\theta}\alpha^2}{\omega^2\beta^2} + \frac{2\omega^2\beta^2}{\omega^2\beta^2}} + \frac{e^{i\theta}\alpha}{\omega\beta}}{\sqrt{\frac{e^{2i\theta}\alpha^2}{\omega^2\beta^2} + \frac{2\omega^2\beta^2}{\omega^2\beta^2}}} - \frac{e^{i\theta\alpha}}{\omega\beta})^2 \times exp\frac{\frac{e^{2i\theta}\alpha}{\omega\beta}\sqrt{\frac{e^{2i\theta}\alpha^2}{\omega^2\beta^2} + \frac{2\omega^2\beta^2}{\omega^2\beta^2}}}{\frac{\omega^2\beta^2}{\omega^2\beta^2}} \tag{69}$$

Let $\frac{e^{i\theta}\alpha}{\omega\beta} = R$

$$\frac{I_2}{I_1} = (\frac{\sqrt{R^2+2} + R}{\sqrt{R^2+2} - R})^2 \times exp(2R\sqrt{R^2+2}) \tag{70}$$